Atmos. Chem. Phys. Discuss., https://doi.org/10.5194/acp-2018-970
Manuscript under review for journal Atmos. Chem. Phys.
Discussion started: 27 September 2018

Atmospheric Chemistry and Physics Discussions

Causes of a continuous summertime O_3 pollution event in Ji'nan, a central city in the North China Plain

Xiaopu Lyu[1], Nan Wang[2], Hai Guo[1*], Likun Xue[3], Fei Jiang[4], Yangzong Zeren[1], Hairong Cheng[5], Zhe Cai[4], Lihui Han[6], Ying Zhou[6]

[1] Department of Civil and Environmental Engineering, The Hong Kong Polytechnic University, Hong Kong, China

[2] Division of Environmental Meteorology， Institute of Tropical and Marine Meteorology， China Meteorology Administration，Guangzhou，China

[3] Environment Research Institute, Shandong University, Ji'nan, China

[4] Jiangsu Provincial Key Laboratory of Geographic Information Science and Technology, International Institute for Earth System Science, Nanjing University, Nanjing, China

[5] Department of Environmental Engineering, School of Resource and Environmental Sciences, Wuhan University, Wuhan, China

[6] Department of Environmental Science, College of Environmental and Energy Engineering, Beijing University of Technology, Beijing, China

* Corresponding author: ceguohai@polyu.edu.hk

Abstract: In summer 2017, measurements of ozone (O_3) and its precursors were carried out at an urban site in Ji'nan, a central city in the North China Plain (NCP). A continuous O_3 pollution event was captured during August 4-11, with the maximum hourly O_3 reaching 154.1 ppbv. The O_3 pollution was associated with the uniform pressure field over the NCP, and was also aggravated by the low pressure trough on August 9-10. Model simulation indicated that local photochemical formation and regional transport contributed 14.0±2.3 and 18.7±4.0 ppbv/hr to O_3 increase during 09:00-15:00 local time (LT), respectively. In the evening, vertical transport dominated the O_3 sources with the contribution of 54.5±9.6 ppbv/hr. For local O_3 formation, the calculated OH reactivity of volatile organic compounds (VOCs) and carbon monoxide (CO) was comparable between O_3 episodes and non-episodes (p>0.05), so was the OH reactivity of

nitrogen oxides (NO_x). However, the ratio of OH reactivity of VOCs and CO to that of NO_x increased from 2.0±0.4 s^{-1}/s^{-1} during non-episodes to 3.7±0.7 s^{-1}/s^{-1} during O_3 episodes, which resulted in the change of O_3 formation mechanism from VOC-limited regime (non-episodes) to transition area (O_3 episodes) where O_3 production rates were among the highest. Correspondingly, the simulated local O_3 production rate during O_3 episodes (maximum: 21.3 ppbv/hr) was markedly higher than that during non-episodes (p<0.05) (maximum: 16.9 ppbv/hr). Given that gasoline and diesel exhaust made great contributions to O_3 precursors and O_3 production rate, constraint on vehicular emissions is the most effective strategy to control O_3 pollution in Ji'nan. Specifically, 10% reduction of diesel and gasoline exhaust led to a decrease of the simulated O_3 production rate of 0.58 and 0.47 ppbv/hr, respectively. Both the observation and model simulation imply that the NCP is a source region of tropospheric O_3, and may "export" photochemical pollution to the surrounding areas.

Keywords: Ozone, local formation, regional transport, volatile organic compound, North China Plain

1 Introduction

Air pollution in the North China Plain (NCP), the largest alluvial plain of China consisting of Beijing, Tianjin and many cities in Hebei, Shandong, and Henan provinces, has attracted much attention of researchers in recent years. While the annual average concentration of $PM_{2.5}$ (particulate matters with aerodynamic diameter less than or equal to 2.5 μm) has been reduced under concerted efforts on emission restrictions (Zhang et al., 2015; Lang et al., 2017), the tropospheric ozone (O_3) pollution, which is less visible than haze but may be equivalently harmful to human health, is still severe. At a regional receptor site of the NCP in a mountainous area north of Beijing, Wang et al. (2006) reported the maximum hourly O_3 of 286 ppbv. A year-round observation of O_3 at 10 urban sites in Beijing also revealed high O_3 concentrations through May to August (Wang et al., 2015a). Hourly O_3 mixing ratios of up to 120 ppbv were reported on Mt. Tai, the highest mountain in the NCP (1534 m a.s.l.) (Gao et al., 2005). This indicates the significant photochemical O_3 pollution over the entire NCP. Moreover, O_3 has been increasing in the NCP during the last decades (Zhang et al., 2014; Zhang et al., 2015). The increase rate of O_3 at an urban site in Beijing from 2005 to 2011 was quantified as 2.6 ppbv/year (Zhang et al., 2014), comparable to that (1.7-2.1 ppbv/year) at Mt. Tai in the summer between 2003 and 2015

(Sun et al., 2016). The severe O_3 pollution in the NCP may not only result from the intensive emissions of precursors but also relate to the synoptic systems and topographic features in this region (Chen et al., 2009; Zhang et al., 2016). For example, the strong photochemical production of O_3 in urban plumes of Beijing was found by Wang et al. (2006), while the contribution of regional transport was revealed by the enhanced O_3 production at a rural site in the NCP under southerly winds (Lin et al., 2008). Through the review of synoptic systems in the NCP from 1980 to 2013, Zhang et al. (2016) concluded that the air quality was generally unhealthy under weak East Asian Monsoons. Moreover, a decadal statistical analysis indicated that meteorological factors explained ~50% of the O_3 variations in Beijing (Zhang et al., 2015). Hence, comprehensive studies on the physical and chemical processes influencing O_3 pollution are urgent in the highly populated and industrialized NCP.

Volatile organic compounds (VOCs), carbon monoxide (CO) and nitrogen oxides (NO_x) are key precursors of tropospheric O_3 (Crutzen, 1973; Chameides and Walker, 1973; Carter, 1994; Carter et al., 1995). The general chemical reactions R(1) - R(5) show the production of O_3 from the OH initiated oxidation of hydrocarbons (RH) (Jenkin et al., 1997; Atkinson, 2000; Jenkin and Clemitshaw, 2000).

$$RH + OH + O_2 \rightarrow RO_2 + H_2O \quad (R1)$$

$$RO_2 + NO \rightarrow RO + NO_2 \quad (R2)$$

$$RO + O_2 \rightarrow Carbonyls + HO_2 \quad (R3)$$

$$HO_2 + NO \rightarrow OH + NO_2 \quad (R4)$$

$$NO_2 + O_2 + h\nu \rightarrow O_3 + NO \quad (R5)$$

The production of O_3 is generally limited by VOCs or NO_x or co-limited by both VOCs and NO_x, depending upon the air profiles, particularly the relative OH reactivity of VOCs and NO_x (OH reactivity is the sum of the products of O_3 precursors concentrations and the reaction rate constants between O_3 precursors and OH). In general, VOCs and NO_x are identified as the limiting reagents in O_3 formation in urban and remote areas, respectively, mainly due to the large quantities of NO_x emissions from vehicles and power plants in cities (Sillman et al., 1990; Shao et al., 2009a). With the aid of a chemical transport model, Liu et al. (2010) indicated that O_3 formation was generally limited by NO_x in most areas of central and western China, and switched from VOC-limited regime in January to NO_x-limited regime in July over eastern China.

Xue et al. (2014) found that O_3 formation was limited by VOCs in Shanghai (East China) and Guangzhou (South China) in spring, and limited by NO_x in Lanzhou (West China) in summer. Alkenes, aromatics and carbonyls can be readily oxidized by oxidative radicals (*e.g.* OH) or photolyzed (applicable for carbonyls), leading to O_3 formation (Cheng et al., 2010; Guo et al., 2013). Therefore, the sources with a bulk emission of these VOCs generally make considerable contributions to the photochemical production of ground-level O_3. For example, O_3 formation at an urban site in Hong Kong was most sensitive to xylenes emitted from solvent usage (Ling and Guo, 2014). Solvent based industry and paint solvent usage with high emissions of aromatics were responsible for more than half of O_3 formation potential in Shanghai (Cai et al., 2010). Carbonyls and alkenes accounted for 71-85% of the total OH reactivity of VOCs in Beijing (Shao et al., 2009b).

In addition to the chemical processes, O_3 pollution is also closely associated with meteorological conditions, which influence the formation, transport and accumulation of O_3. Studies (Chan and Chan, 2000; Huang et al., 2005) indicated that tropical cyclone (typhoon) and continental anticyclone are the most common synoptic systems conducive of O_3 pollution in coastal cities of southern China. Many O_3 episodes in eastern China occurred under the control of the west Pacific subtropical high pressure (He et al., 2012; Shu et al., 2016). In the NCP, the summertime O_3 pollution is generally accompanied with a weak high pressure system (Wang et al., 2010). Furthermore, the terrain also plays a role in O_3 pollution. For example, the mountains in north and west of Beijing lead to upslope winds (valley breeze) in daytime, transporting polluted air masses laden with O_3 from NCP to Beijing (Lin et al., 2008). Overall, the causes of O_3 pollution are generally complicated and need to be analyzed case by case.

Ji'nan, the capital of Shandong province, also suffers from heavy photochemical pollution. As early as 2000s, studies (Shan et al., 2008; Yin et al., 2009) reported the maximum hourly O_3 of 143.8 ppbv and 147.8 ppbv in June 2004 and 2005, respectively. Even higher O_3 (198 ppbv) was observed at a rural site downwind of Ji'nan in June 2013 (Zong et al., 2018). Given that O_3 is continuously increasing in China, O_3 pollution in Ji'nan needs to be investigated in detail. On one hand, Ji'nan is an important city in Shandong Peninsula with a high population density. The O_3 pollution in Ji'nan is a concern of local residents. On the other hand, Ji'nan is a good example representing the medium-sized cities in the NCP with dense population, intensive industrial

emission and outdated production capacity. It has been repeatedly confirmed that air pollution in these types of cities in the NCP has seriously deteriorated air quality in Beijing (Lin et al., 2008; Wang et al., 2010). Thus, O_3 pollution in Ji'nan is also a regional issue. Contradictory to the critical roles of the cities like Ji'nan in the NCP and the necessity of O_3 studies, our knowledge on O_3 pollution in the NCP (except for Beijing and Tianjin) is rather limited. To better understand O_3 pollution in the NCP, this study investigated the causes of an O_3 episode lasting for eight days in Ji'nan in the summer of 2017. The analyses presented here focus on the synoptic systems dominating Shandong Peninsula during this event; the chemical profiles of O_3 and O_3 precursors; and the simulation of factors contributing to O_3 in Ji'nan with the aid of a chemical transport model and a photochemical box model. In addition, we propose feasible O_3 control measures based on the source-resolved OH reactivity of VOCs and NO_x.

2 Methodology

2.1 Site description

The air quality monitoring and sample collection were carried out on the rooftop of a 7-story building on the campus of Shandong University from July 15 to August 14, 2017. The campus is located in the urban area of Ji'nan, and the site is about 50 m from a main road (Shanda South Road) outside the campus. Figure 1 shows the locations of the sampling site (36.68 °N, 117.07 °E, 22 m a.g.l.) and some surrounding urban air quality monitoring stations (AQMSs) set up by China National Environmental Monitoring Center (CNEMC). Also shown are the observed O_3 and monitored rainfall averaged over August 4-11, 2017 when O_3 episodes occurred in Ji'nan. It is noteworthy that the days with maximum hourly O_3 exceeding 100 ppbv (Grade II of National Ambient Air Quality Standard) were defined as O_3 episode days. O_3 data in hourly resolution at the AQMSs were obtained from the website of CNEMC (http://www.cnemc.cn/).

Atmos. Chem. Phys. Discuss., https://doi.org/10.5194/acp-2018-970
Manuscript under review for journal Atmos. Chem. Phys.
Discussion started: 27 September 2018

Atmospheric Chemistry and Physics Discussions

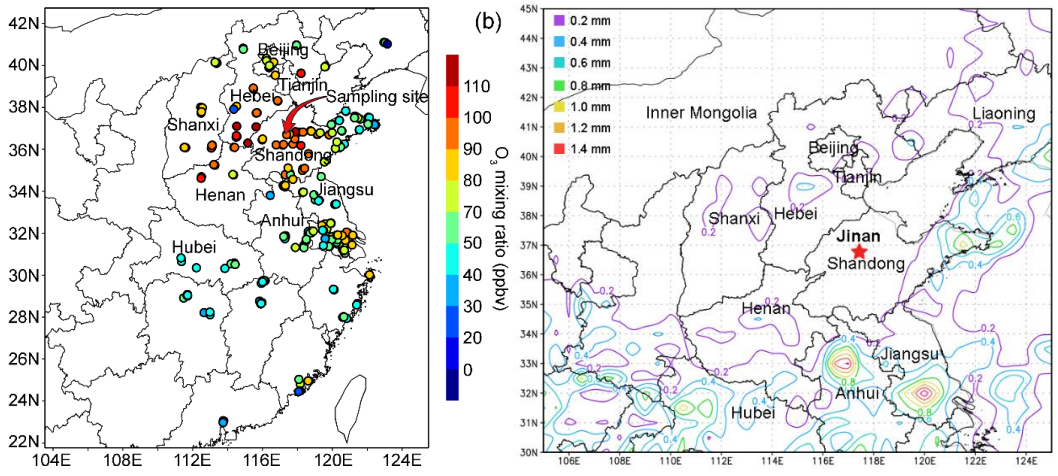

Figure 1 Locations of the sampling site and the CNEMC AQMSs (colored circles in the left panel). Left panel color scale: Observed O_3 at 14:00 LT averaged over August 4-11, 2017. The location of the sampling site is overlapped with the nearest AQMS in Ji'nan. Right panel: Rainfall distribution, in millimeters (mm), averaged over August 4-11, 2017.

2.2 Air quality monitoring and sample collection

2.2.1 Continuous monitoring of air pollutants and meteorological parameters

O_3, NO and NO_2 were continuously monitored at the sampling site between July 15 and August 14, 2017. The air was drawn through a 4 m Teflon tube by the pumps in the trace gas analyzers with the total flow rate of 2 L/min (1.4 L/min for O_3 analyzer and 0.6 L/min for NO_x analyzer). The inlet was located ~1 m above the rooftop of the 7-story building (~22 m a.g.l.). O_3 and NO/NO_x were detected with a UV photometric based analyzer and a chemiluminescence NO-NO_2-NO_x analyzer, respectively. NO_2 was calculated from the difference between NO and NO_x. Studies indicated that NO_2 monitored with chemiluminescence was generally overestimated due to the conversion of other nitrogen containing compounds to NO by molybdenum oxide catalysts (McClenny et al., 2002; Dunlea et al., 2007; Xu et al., 2013). The positive interference is more significant in more aged air masses where peroxyacetyl nitrate (PAN), nitric acid (HNO_3) and alkyl/ multifunctional alkyl nitrates (ANs) are abundant (Dunlea et al., 2007). The average overestimation of NO_2 was 22% in Mexico City, which even increased to 50% in the afternoon (Dunlea et al., 2007). Though comparable or even higher overestimations were identified at the

suburban and mountainous sites in China, Xu et al. (2013) suggested that the chemiluminescence monitors overestimated NO_2 by less than 10% in urban areas with fresh emission of NO_x. As described in section 2.1, our sampling site was located in the urban area of Ji'nan and was only ~50 m to a main road. Therefore, we infer that NO_2 might not be significantly overestimated in this study. However, the influences of the overestimation on the findings were still discussed qualitatively where necessary.

The hourly concentrations of sulfur dioxide (SO_2) and CO were acquired from a nearest AQMS of CNEMC which is ~1 km from our sampling site. Year-round monitoring of inorganic trace gases was conducted at this AQMS, where the air was drawn into the analytical instruments at a flow rate of 3 L/min through an inlet, ~1 m above the rooftop of a 5-story building (~ 16 m a.g.l.). Table S1 provides the details of the trace gas analyzers used in this study, including the instrumental model, resolution, accuracy, precision and detection limit. The hourly concentrations of O_3 and NO_2 (NO data was not available on CNEMC website) measured at our sampling site agreed well with those reported at the AQMS, with the slope of 1.04 (R^2 = 0.82) and 1.13 (R^2 = 0.71) for O_3 and NO_2 in the linear least square regressions, respectively (Figure S1). Due to the instrumental differences and/or differences in sources and sinks of air pollutants at the two sites, the agreements were worse at low mixing ratios for both O_3 and NO_2. Therefore, we only used SO_2 and CO monitored at the nearest AQMS in this study, which had lower photochemical reactivity than O_3 and NO_2, and might be more homogeneous at a larger scale.

In addition, the meteorological parameters, including wind speed, wind direction, pressure, temperature and relative humidity were monitored by a widely used weather station (China Huayun group, Model CAWS600). The daily total solar radiation was obtained from the observations at a meteorological station in Ji'nan (36.6 °N, 117.05 °E, 170.3 m a.s.l), 9 km to our sampling site.

2.2.2 Sample collection and chemical analysis

During the real-time measurement of trace gases, offline VOC and oxygenated VOC (OVOC) samples were collected on 9 selective days (*i.e.*, July 20 and 30, August 1, 4-7 and 10-11), referred to as VOC sampling days hereafter. The days were selected to cover the periods with relatively high and low levels of O_3. The high O_3 days were forecasted prior to sampling based on the numerical simulations of meteorological conditions and air quality. In total, 6 out of 9

VOC/OVOC sampling days were O_3 episode days with the maximum hourly O_3 ranging from 100.4 to 154.1 ppbv. On each day (regardless of episode or non-episode), 6 VOC/OVOC samples were collected between 08:00 and 18:00 local time (LT) every 2 hours with the duration of 1 hour for VOC and 2 hours for OVOC samples. VOC samples were collected with 2 L stainless steel canisters which were cleaned and evacuated before sampling. A flow restrictor was connected to the inlet of the canister to guarantee 1 hour sampling. OVOC were sampled with the 2,4-dinitrophenylhydrazine (DNPH) cartridge, in front of which an O_3 scrubber was interfaced to remove O_3 in the air. A pump behind the DNPH cartridge drew the air at a flow of 500 L/min. After sampling, all the DNPH cartridges were stored in a refrigerator at 4 $^{\circ}$C until chemical analysis.

VOC samples were analyzed with a gas chromatograph-mass selective detector/flame ion detector/electron capture detector system (Colman et al., 2001). In total, 85 VOCs, including 59 hydrocarbons, 19 halocarbons and 7 alkyl nitrates, were quantified. The overall ranges of the detection limit (DL), accuracy and precision for VOCs analysis were 1-154 pptv, 1.2-19.8% and 0.1-17.9%, respectively. The analysis results given by this system have been compared with those analyzed by UCI and good agreements were achieved (Figure S2). OVOC samples were eluted with 5 mL acetonitrile, followed by analysis with the high performance liquid chromatography. The DL, accuracy and precision for all OVOCs analysis were within the range of 3-11 pptv, 0.32-0.98% and 0.01-1.03%, respectively.

2.3 Model configuration

2.3.1 Chemical transport model

To analyze the processes contributing to high O_3 in Ji'nan, a chemical transport model, the Weather Research Forecast-Community Multi-scale Air Quality (WRF-CMAQ), was utilized to simulate O_3 in this study. WRF v3.6.1 was run to provide the offline meteorological field for CMAQ v5.0.2. A two-nested domain was adopted with the resolution of 36 km (outer domain) and 12 km (inner domain), respectively. As shown in Figure S3, the outer domain covered the entire continental area of China aiming to provide sufficient boundary conditions for the inner domain, which specifically focused on eastern China.

We used the 2012-based Multi-resolution Emission Inventory for China (MEIC) to provide anthropogenic emissions of air pollutants, which was developed by Tsinghua University specific for China, with the grid resolution of 0.25 °×0.25 ° (Zhang et al., 2007; He, 2012). Five emission sectors, namely transportation, agriculture, power plant, industry and residence were included in MEIC. The emission inventory was linearly interpolated to the domains with consideration of the earth curvature effect. For grids outside China, the air pollutant emissions were derived from INTEX-B (Intercontinental Chemical Transport Experiment-Phase B) Asian emission inventory (Zhang et al., 2009). Consistent with many previous studies (Jiang et al., 2010; Wang et al., 2015b), the Model of Emissions of Gases and Aerosols from Nature (MEGAN) was used to calculate the natural emissions. The physical and chemical parameterizations for WRF-CMAQ were generally identical to those described in Wang et al. (2015b), with some improvements. Firstly, the carbon bond v5 with updated toluene chemistry (CB05-TU) was chosen as the gas phase chemical mechanism (Whitten et al., 2010). Secondly, a single-layer urban canopy model (Kusaka and Kimura, 2004) was used to model the urban surface-atmosphere interactions. Thirdly, the default 1990s U.S. Geological Survey data in WRF was replaced by adopting the 2012-based moderate resolution imaging spectroradiometer (MODIS) land cover data for eastern China. The substitution was performed to update the simulation of boundary meteorological conditions (Wang et al., 2007).

An integrated process rate (IPR) module incorporated in CMAQ was used to analyze the processes influencing O_3 concentration. Through solving the mass continuity equation established between the overall change of O_3 concentration with time and the change of O_3 concentration caused by individual processes, including horizontal diffusion (HDIF), horizontal advection (HADV), vertical diffusion (VDIF), vertical advection (VADV), dry deposition (DDEP), net effect of chemistry (CHEM) and cloud processes (CLD), the contributions of the processes to O_3 variation rate were determined. Note that the estimate of CHEM is influenced by the estimate of O_3 precursor emissions, the simulation of meteorological conditions and the chemical mechanism, all the three aspects should be taken into account wherever CHEM is discussed. The IPR analysis has been widely applied in process diagnosis of O_3 pollution (Huang et al., 2005; Wang et al., 2015b).

2.3.2 Photochemical box model

A Photochemical Box Model incorporating the Master Chemical Mechanism (PBM-MCM) was used to study the in situ O_3 chemistry, in view of the detailed (species-based) descriptions of VOC degradations in the MCM (Saunders et al., 2003; Lam et al., 2013). The PBM model was localized to be applicable in Ji'nan, with the settings of geographic coordinates, sunlight duration and photolysis rates. The photolysis rates were calculated by the TUV model (Madronich and Floke, 1997). Specifically, the geographical coordinates, date and time were input into the TUV model, initializing the calculation of solar radiation with the default aerosol optical depth (AOD), cloud optical depth (COD), surface albedo and other parameters. Then, COD was adjusted to make the calculated daily total solar radiation progressively closer to the observed value. When the difference between the calculated and observed solar radiation were less than 1%, the input parameters with the adjusted COD were accepted. Based on the settings, the hourly solar radiations and the photolysis rates of O_3 ($J(O^1D)$) and NO_2 (JNO_2) were calculated by the TUV model, and applied to PBM-MCM for O_3 chemistry modelling. Table S2 shows the daily maximum $J(O^1D)$ and JNO_2 on the VOC sampling days. The MCM v3.2 (http://mcm.leeds.ac.uk/MCM/) used in the present model consists of 17,242 reactions among 5,836 species. The measurements of O_3 and its precursors at 00:00 on each day were used as the initial conditions for each day's modelling. The initial O_3, as the O_3 left over from the days before the modelling day, accounted for a part of the primary OH production. Hourly concentrations of 46 VOCs, 4 OVOCs and 4 trace gases (SO_2, CO, NO and NO_2), as well as hourly meteorological parameters (temperature and relative humidity) were input into the model, so that the model was constrained to observations. The hourly observed O_3 were not input, as it was the species to be modeled. The Freon, cycloalkanes and methyl cycloalkanes with low O_3 formation potentials were not included in model input. Also omitted were the species whose concentrations were lower than the detection limits in more than 20% of the samples, such as the methyl hexane and methyl heptane isomers. For the hours when measurement data were not available, the concentrations were obtained with linear interpolation. Some secondary species, such as formaldehyde (HCHO), acetaldehyde and acetone, were input into the model to constrain the simulation. Since other secondary species, *e.g.*, PAN and HNO_3 were not observed in this study, their concentrations were calculated by the model. Dry deposition was considered for all the chemicals by setting the deposition velocities identical to those in Lam et al. (2013). Since

NO and NO_2 were separately measured and input into the model, which experienced different reactions as described by the species-based chemical mechanisms.

The simulations were separately carried out on all the VOC sampling days. To spin-up the model, the concentrations of air pollutants and meteorological conditions which were the same as those on the day of interest were input into the model for 72-h simulation before the modelling on that day. The model treated the air pollutants to be well-mixed in the boundary layer, without consideration of dilution and transport. O_3 in the free troposphere was not considered either, due to the lack of O_3 observations above the boundary layer over Ji'nan. This might hinder the accurate reproduction of the observed O_3, particularly on the days when advection and diffusion were strong. Since the model mainly described the in situ photochemistry, it was validated through comparison with the CHEM process simulated by WRF-CMAQ. The simulated O_3 production rates were output every hour, which were integrated values over every 3600 s (model resolution: 1 s). More details about the model configuration can be found in Lam et al. (2003) and Lyu et al. (2017).

2.3.3 Positive Matrix Factorization (PMF) model

PMF was employed to identify the sources of O_3 precursors. Details about the operation principles of PMF can be found in Paatero and Tapper (1994). Briefly, the model treats the matrix of input concentrations as the product of two matrixes (*i.e.*, factor contribution and factor profile). Here, hourly concentrations of 31 VOCs, CO, NO and NO_2 in 54 samples were input into the model. The VOCs, which were common tracers of specific sources (*e.g.*, isoprene for biogenic emissions), and had relatively high concentrations (detectable in at least 80% samples), were selected for source apportionment (termed as VOCs* hereafter). On average, VOCs* accounted for 79.5±11.7% of the total quantified VOCs (mean ± 95% confidence interval of the hourly values in the statistical period, same for all the other "a ± b" expressions elsewhere unless otherwise specified). The uncertainties of the input concentrations of O_3 precursors were set as $\frac{5}{6} \times$ DL and $\sqrt{(10\% \times concentration)^2 + (0.5 \times DL)^2}$ for the concentrations lower than and higher than DL, respectively.

The model was run for 20 times with a random seed and the best resolution automatically given by the model was accepted. A total of 6 sources of O_3 precursors were resolved by PMF in this

study. The number of sources was chosen based on the criteria that the tracers indicating different sources were not allocated in the same source, and all the sources were interpretable according to the tracers. The Bootstrap method integrated in PMF was used to estimate the uncertainties of the modelling results.

3. Results and discussion

3.1 Overall characteristics of O_3 pollution in Ji'nan

Figure 2 shows the time-dependent variations of trace gases, the calculated OH reactivity of VOCs, CO and NO_x, and meteorological conditions on the VOC sampling days in Ji'nan (Hourly values of trace gases in the whole sampling period are shown in Figure S4). The OH reactivity of O_3 precursors instead of their absolute concentrations was analyzed in this study, because OH reactivity, which considers both the abundances of precursors and reaction rate constants between different precursors and OH, more appropriately indicates the potentials of different precursors in contributing to O_3 production. It should be kept in mind that OH reactivity still does not reflect the actual contributions of O_3 precursors to O_3 production, unlike what the box model is capable of (McDuffie et al., 2016). As shown in Figure 2, the OH reactivity of VOCs are grouped into those of carbonyls, biogenic VOCs (BVOCs), aromatics, alkenes and alkanes (Table S3 lists the VOC species included in these groups). The reaction rate constants between O_3 precursors and OH in calculation of OH reactivity were adopted from the MCM v3.2 (http://mcm.leeds.ac.uk/MCM/). The average total OH reactivity on VOC sampling days ($19.4 \pm 2.1\ s^{-1}$) was comparable to that reported in New York ($19 \pm 3\ s^{-1}$, Ren et al., 2003), Houston ($9\text{-}22\ s^{-1}$, Mao et al., 2010) and Beijing ($15\text{-}27\ s^{-1}$, Williams et al., 2016). Consistent with the previous studies in urban areas (Ren et al., 2003; Yang et al., 2016 and references therein), NO_x was the largest contributor (28.9±1.9%) to the total OH reactivity. Noticeably, 20.5±4.1% of the total OH reactivity was attributable to BVOCs, which was much higher than the contributions in urban areas (<10%) reviewed by Yang et al. (2016). The elevated isoprene level (1.5±0.2 ppbv) under high temperature (mean: 31 °C) might explain the considerable contribution of BVOCs to the total OH reactivity in this study.

According to Figure 2, the first three days were non-episodes, while the rest were all O_3 episodes with the highest O_3 of 154.1 ppbv at 13:00 LT on August 10. It was found that the total OH reactivity of VOCs and CO ($OH\ reactivity_{VOCs+CO}$) was comparable between O_3 episodes

(14.8±2.0 s^{-1}) and non-episodes (12.2±3.0 s^{-1}), so was the OH reactivity of NO_x (4.7±0.8 s^{-1} and 6.9±1.9 s^{-1} during episodes and non-episodes, respectively). Throughout the text, the statistics were averages of hourly values over the period of interest when comparisons were made unless otherwise specified. Here, the OH reactivity of VOCs and CO was considered together as their reactions with OH generally lead to O_3 production, in contrast to the anti-correlation between NO_x and O_3 in VOC-limited regime due to the depletion of OH by NO_2 ($OH + NO_2 \rightarrow HNO_3$). Since NO_2 might be more overestimated on episode days due to the higher concentrations and greater interferences of HNO_3, PAN and ANs, the actual OH reactivity of NO_x during episodes might be lower than that during non-episodes. In fact, the high OH reactivity during non-episodes was mainly caused by high concentrations of O_3 precursors on July 30 and August 1. As shown in Figure 2, the highest pressures (color of the wind vectors) throughout the sampling campaign were observed on these two days, which might suppress the dispersion of O_3 precursors. More importantly, the solar radiation was relatively weak and the temperature was low, particularly on July 30 when the maximum solar radiation and highest temperature was only 244 W/m^2 and 26.2 ℃, respectively. This meant that photochemical consumption of O_3 precursors might be weakened on these days, causing the high OH reactivity of O_3 precursors. Despite comparable OH reactivity between episodes and non-episodes, we found that the ratio of $\frac{OH\ reactivity_{VOCs+CO}}{OH\ reactivity_{NOx}}$ during O_3 episodes (3.7±0.7 s^{-1}/s^{-1}) was higher (p<0.05) than during non-episodes (2.0±0.4 s^{-1}/s^{-1}). Taking into account the greater overestimation of NO_2 on episode days, the difference of $\frac{OH\ reactivity_{VOCs+CO}}{OH\ reactivity_{NOx}}$ between episodes and non-episodes might be even larger. This indicated that O_3 formation was more limited by VOCs during non-episodes than during episodes. In fact, O_3 formation in Ji'nan switched to the transition area during episodes from the VOC-limited regime during non-episodes (see section 3.4.2). This might partially explain the building-up of O_3 on episode days, as O_3 production was generally the highest in the transition area. The contribution of BVOCs to total OH reactivity during O_3 episodes (24.0±5.7%) was much higher than during non-episodes (13.9±3.6%), which was likely due to more intensive isoprene emissions under stronger solar radiation and higher temperature during episodes (isoprene: 2.2±0.6 ppbv during episodes and 0.9±0.3 ppbv during non-episodes). Many studies have found that BVOCs are efficient O_3 producers due to their abilities to propagate radicals (Curci et al., 2009; Cheng et al., 2010). Keep in mind that the abundances of O_3 precursors were

368 also influenced by the meteorological conditions, in addition to emissions. We do not claim that
369 the change of $\frac{OH\ reactivity_{VOCs+CO}}{OH\ reactivity_{NOx}}$ was merely attributable to variations in emissions.

370 SO_2 and CO were higher during non-episodes than during episodes (p<0.05), due to the
371 accumulation of primary air pollutants on July 30 and August 1. While NO and NO_2 were
372 respectively comparable between non-episodes and O_3 episodes (p>0.05), the ratio of NO_2/NO
373 increased substantially from 1.7±0.3 ppbv/ppbv during non-episodes to 3.0±0.4 ppbv/ppbv
374 during episodes (p<0.05). This was likely attributable to more conversion of NO to NO_2 under
375 higher levels of O_3 and peroxy radials during episodes, when the stronger solar radiation played
376 an important role in enhancing the formation of O_3 and peroxy radicals. Nevertheless, the higher
377 average ratio of NO_2/NO on episode days was partially caused by the greater overestimation of
378 NO_2 during episodes.

379 From the perspective of meteorological conditions, O_3 episodes had relatively stronger solar
380 radiation, higher temperature, lower relative humidity and weaker winds (p<0.05). This is
381 reasonable as O_3 formation and accumulation are generally enhanced under these weather
382 conditions. As aforementioned, the solar radiation on July 30 was much weaker than those
383 during O_3 episodes, which was probably the most critical factor leading to low O_3 on this day.
384 Figure S5 shows the COD retrieved from the terra/MODIS (https://ladsweb.modaps.
385 eosdis.nasa.gov/search/imageViewer/1/MOD06_L2--61/2017-08-06/DB/Site:142/2873994172--
386 3) at 10:00 – 12:00 (local time) of the VOC sampling days. The terra/MODIS image revealed
387 thick cloud cover with high COD over Ji'nan on July 30, explaining the weak solar radiation. In
388 fact, obvious anti-correlation existed between solar radiation and the COD. The influences of
389 cloud cover/ COD and solar radiation on O_3 pollution during the study period in Ji'nan are
390 discussed in section 3.2. Unlike many previous findings that O_3 pollution was aggravated by high
391 pressure (Chan and Chan, 2000; Zhao et al., 2009), the sea-level pressure during O_3 episodes
392 (993.4±0.2 hPa) was significantly lower than during non-episodes (996.1±0.4 hPa) in this study
393 (p<0.05). When O_3 reached its hourly maximum on August 10 (154.1 ppbv), the pressure was at
394 its lowest value of the campaign (990.2 hPa). The continuously severe O_3 pollution event under
395 low pressure is further investigated below.

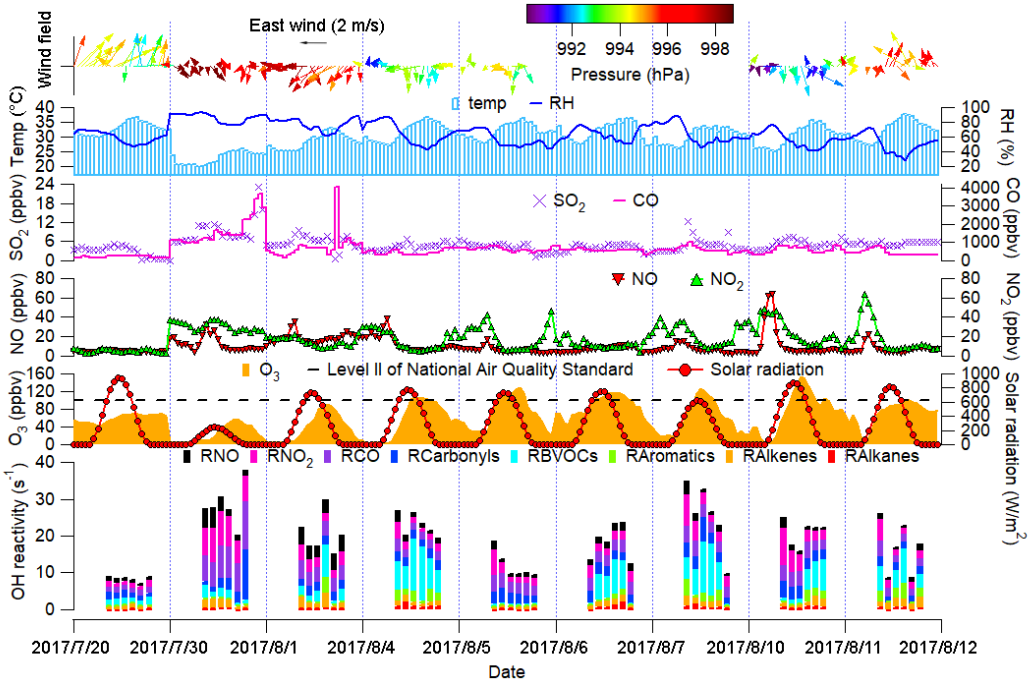

Figure 2 Time-dependent variations of trace gases, OH reactivity of O_3 precursors and meteorological parameters. Wind speed and wind direction were not monitored from 17:00 LT on August 5 to 23:00 LT on August 7 due to malfunction of the weather station. RX in the bottom panel is the OH reactivity of species/group X.

3.2 Synoptic processes and relationship with O_3 pollution

Figure 3 displays the average weather charts at 14:00 LT during O_3 episodes and non-episodes (weather charts on individual VOC sampling days are shown in Figure S6). Clearly, the temperature over Shandong Peninsula was much higher during O_3 episodes than non-episodes, which favored O_3 formation on episode days. Additionally, southerly and southwesterly winds originating from the inland areas (Hubei, Henan, and Anhui provinces) prevailed in central and western Shandong province during O_3 episodes. In contrast, the winds were generally from the sea or coastal region in Jiangsu province during non-episodes. O_3 and O_3 precursors might be transported to Ji'nan in the former cases. For the latter cases, though the winds were from relatively the clean sea and coastal region, the concentrations of O_3 precursors on July 30 and August 1 (non-episode days) were still high, which were mainly caused by weather conditions

Atmos. Chem. Phys. Discuss., https://doi.org/10.5194/acp-2018-970
Manuscript under review for journal Atmos. Chem. Phys.
Discussion started: 27 September 2018

Atmospheric Chemistry and Physics Discussions

(high pressure, low temperature and low solar radiation), as discussed in section 3.1. Nevertheless, we believe that the incoming sea and coastal air at least did not aggravate air pollution in Ji'nan during non-episodes, including on July 30 and August 1. Further, we also noted that the winds changed direction from southwest to northwest around Ji'nan during O_3 episodes. This meant that there might be a local circulation hampering the dispersion of air pollutants during episodes. Overall, the wind fields were more favorable for regional transport and accumulation of air pollutants in Ji'nan during episodes. It seems that the turning-round of the winds around Ji'nan was associated with the sea breeze from Bohai Bay, which might be one of the typical factors influencing air pollution in the Shandong Peninsula, like the convergence of continental air and sea breeze (from South China Sea) in Hong Kong (Fung et al., 2005; Lo et al., 2006). Unlike the weak mesoscale sea breezes originating from Bohai Bay during episodes, the synoptic winds from the open sea swept over the Shandong Peninsula and did not converge with the continental air during non-episodes, thus not a factor aggravating air pollution in Ji'nan.

In addition, Ji'nan was on the peripheral of a high pressure system over the Yellow Sea during non-episodes, which might drive the clean and humid oceanic air to Ji'nan. In contrast, Shandong Peninsula was under a uniform pressure field with the sea-level pressure of 1000-1001 hPa during O_3 episodes, implying the relatively stagnant weather conditions unfavorable for the dispersion of air pollutants.

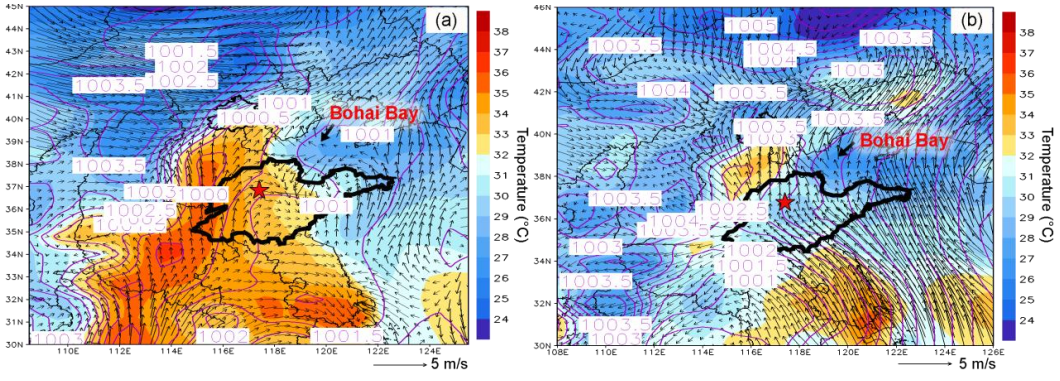

Figure 3 Weather chart at 14:00 LT averaged over (a) O_3 episodes and (b) non-episodes. The red star represents Ji'nan. The dark black line is the boundary of Shandong province. Bohai Bay is located to the northeast of Shandong province. Numbers in the figure are sea-level pressures in unit of hPa.

To better understand the relationship between O_3 pollution and the synoptic systems, Table 1 summarizes the characteristics of synoptic system, weather condition and air mass origin on individual VOC sampling days. The weather charts for the surface level and 500 hPa on August 1, 4, 7, 10 and 13 are presented in Figures S6-S7, which showed the evolution of synoptic systems at different stages of the O_3 episodes. To identify the origins of air masses, the 48 hour backward trajectories of air masses are shown in Figure 4. The trajectories were computed using the Hybrid Single Particle Lagrangian Integrated Trajectory (HYSPLIT) Model v 4.9. Each trajectory was calculated for 48 hours and the calculation was done every 6 hours (4 trajectories each day). Our sampling site (36.68 °N, 117.07 °E) was set as the starting point of the backward trajectories with the height of 500 m a.s.l. The discrepancy between the wind direction and origin of air masses, *e.g.* on August 1 and 11, was likely due to the air recirculation at the ground level.

It was found that Ji'nan was under the control of a Western Pacific Subtropical High pressure system (WPSH) on July 20 (weather chart on 500 hPa is not shown here), and the air masses arriving in Ji'nan originated from South China 48 hours prior (Figure 4). As anticipated, the WPSH caused high temperatures and the intensive solar radiation during the study period (maximum: 943 W/m^2) in Ji'nan (Figure 2), which was conducive to O_3 formation. However, the winds on July 20 were the strongest in the entire VOC sampling period, with the highest hourly wind speed of 3.9 m/s. The strong winds might facilitate the transport and dispersion of O_3 precursors and locally formed O_3 on July 20 (refer to the low levels of O_3, O_3 precursors and OH reactivity in Figure 2).

On July 30 and August 1, the WPSH moved southward and Ji'nan was under a uniform pressure field. The uniform pressure field was formed because Ji'nan was on the periphery of two low pressure systems (two rain belts as shown in Figure 1), *i.e.* one over Central China and another over North China (Figure S7). Thus, the pressure in Ji'nan was relatively high (997.1 ±0.3 hPa), compared to the south and north regions, which was defined as weak high pressure. This synoptic system lasted for several days until August 7, covering 2 non-episode days and 4 O_3 episode days. On July 30, Ji'nan featured very weak solar radiation (maximum: 244 W/m^2) and thick cloud cover (Figure 2 and Figure S5). The weak solar radiation might be primarily responsible for the low O_3 in Ji'nan on July 30. Though there was still some cloud cover over Ji'nan on August 1, the COD decreased relative to that on July 30 (Figure S5). Correspondingly,

the solar radiation increased to the level comparable to that on the O_3 episode days. As a result, the hourly maximum O_3 increased to 90.6 ppbv on August 1, though it was still an O_3 attainment day. In addition, the temperature was relatively low on July 30 and August 1. Though the OH reactivity of O_3 precursors on these days was comparable to or even higher than that on August 4-7 (Figure 2), the weak solar radiation and/or low temperature might not be conducive to O_3 formation which explained the low O_3 on these days. In contrast, continuously strong solar radiation with low COD (Figure 2 and Figure S5), high temperature and continental air masses (Figure 4) were observed on August 4-7, partially accounting for the consecutive O_3 pollution days. In addition, despite the moderate levels of OH reactivity of O_3 precursors on August 4-7, the higher ratio of $\frac{OH\ reactivity_{VOCs+CO}}{OH\ reactivity_{NOx}}$ enabled stronger O_3 production on these days (see sections 3.1 and 3.4.2).

On August 10, the rain belt over North China moved southward, forming a deep low pressure trough over the NCP (Figure S8 (d)). Ji'nan was behind the trough, indicating that there was strong downward air flow in Ji'nan on August 10. It is well known that low pressure trough is a typical synoptic system aggravating O_3 pollution, due to the downward air flow behind the trough, which may bring O_3 in the stratosphere and/or the upper troposphere to the ground (Chan and Chan, 2000). Moreover, there was nearly no cloud cover over the entire NCP on this day (Figure S5), causing strong solar radiation (maximum: 879 W/m^2, only second to those on July 20). Consequently, the highest O_3 (154.1 ppbv) in this sampling campaign was observed on August 10. In addition, the in situ O_3 production rate on this day was higher than on the non-episode days, even under the same meteorological conditions as those during non-episodes, due to the switch of O_3 formation mechanism from VOC-limited regime to transition regime (see section 3.4.2). On August 11, the low pressure system continued to extend to the Yellow Sea. O_3 decreased substantially on this day with the disappearance of the low pressure trough and the weakening of solar radiation, though the hourly maximum O_3 still reached 100.4 ppbv. On the following days, it was rainy in Ji'nan and O_3 decreased to low levels (Figure S4).

Table 1 Summary of the synoptic systems, weather conditions and air mass origins on VOC sampling days.

Date	O_3 maximum	Episode/non-episode	Synoptic system Weather condition	Air mass origin

	(ppbv)			
July 20, 2017	71.0	Non-episode	Subtropical high, strong southwesterly winds	Continental air masses from South China
July 30, 2017	57.6	Non-episode	Uniform pressure field (weak high pressure), rain, fog, calm winds	Marine air masses
August 1, 2017	90.6	Non-episode	Uniform pressure field (weak high pressure), northeasterly winds	Marine air masses
August 4, 2017	107.5	Episode	Uniform pressure field (weak high pressure), northeasterly winds	Continental air masses from Shandong province
August 5, 2017	128.2	Episode	Uniform pressure field (weak high pressure), calm winds	Continental air masses from Shandong province
August 6, 2017	116.9	Episode	Uniform pressure field (weak high pressure), southwesterly winds	Continental air masses mostly from Shandong province
August 7, 2017	126.9	Episode	Uniform pressure field (weak high pressure), calm winds	Continental air masses from the north
August 10, 2017	154.1	Episode	Low-pressure trough, calm winds	Continental air masses from the west
August 11, 2017	100.4	Episode	Subtropical high, southeasterly winds	Continental air masses from the southwest

493

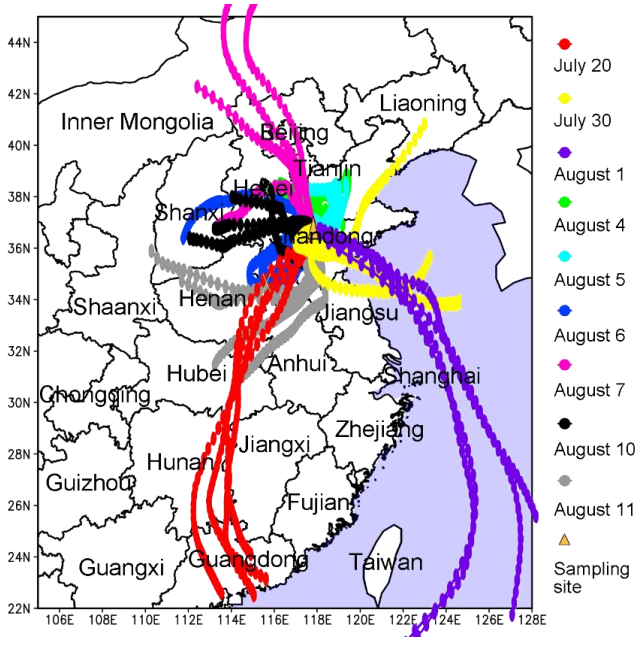

Figure 4 Forty eight hour backward trajectories calculated every 6 hours, with Ji'nan (36.68 °N, 117.07 °E, 500 m a.g.l.) as the starting point. The trajectories are simulated by HYSPLIT v4.9. The water areas are highlighted in blue.

3.3 O_3 simulation and process analysis

To further clarify the causes of the continuous O_3 episodes in Ji'nan, WRF-CMAQ was utilized to simulate O_3 and the processes influencing O_3 concentrations. Figure 5 shows the hourly average simulated and observed O_3 on the VOC sampling days in Ji'nan. Overall, the model well reproduced the magnitudes and diurnal patterns of the observed O_3, except for the higher simulated O_3 on July 20 and the under-prediction of O_3 on August 1, 7 and 10. Due to inevitable uncertainties inherent in the chemical transport models, such as the uncertainties in emission inventory, meteorological simulation and chemical mechanisms (Hu et al., 2016), it is difficult to deduce the reasons for the discrepancies. However, the observation data revealed extremely high levels of some VOCs on the three days when O_3 was under-predicted. Specifically, 13.5 ppbv of ethene was observed at 14:00 LT on August 1. On August 7, 5.6 ppbv of isoprene, 16.2 ppbv of HCHO and 2.3 ppbv of hexanal were measured during 12:00 – 14:00 LT. On August 10, 22.7 ppbv of propene and 12.7 ppbv of *i*-butane were recorded at 08:00 and 16:00 LT, respectively. It

511 is noteworthy that these mixing ratios were 5 – 10 times higher than their averages. Further, most
512 of these VOCs are highly reactive in O_3 photochemistry and may make great contributions to
513 local O_3 production. With the setting of constant emissions of O_3 precursors, WRF-CMAQ did
514 not reproduce these extremely high levels of VOCs, which was a plausible reason for the under-
515 prediction of O_3 on August 1, 7 and 10. Ji'nan was behind a low pressure trough on August 9 –
516 10. However, vertical transport was simulated to make negative contributions to O_3 between
517 10:00 LT and 18:00 LT, according to the process analysis. In addition, the simulated O_3 in the
518 upper atmosphere on August 10 was relatively low compared to that on August 5, 6 and 9
519 (Figure S9). Namely, the model might fail to reproduce the O_3 enhancement driven by the low
520 pressure trough on August 10.

521 The process analysis indicated that horizontal and vertical transport dominated the sources of O_3
522 at noon (10:00-12:00 LT) and the other times of July 20, respectively. While vertical transport
523 might explain the high O_3 at night (Figure 2), it was not likely that horizontal transport built up
524 O_3 at noon, because the southwesterly airflow originated from South China and passed central
525 China (Figure 4) where O_3 values were relatively low on that day (high O_3 occurred in Hebei
526 province in the northwest). Therefore, the overestimate of the transport effect led to the higher
527 simulated O_3 on July 20.

528 Despite these discrepancies, overall the observed O_3 at the sampling site was well reproduced. In
529 addition, the spatial distribution of the simulated O_3 was highly consistent with the observed O_3
530 distribution, as shown in Figure 6. The average concentrations of the simulated VOCs were also
531 compared with the observations (Figure S10). While the day-to-day and diurnal variations of the
532 observed VOCs were not well reproduced (not shown), which is a proverbial drawback of the
533 WRF-CMAQ, the model reasonably simulated the magnitudes of VOCs. Moreover, the averages
534 of the observations (Avg. Obs.) and simulations (Avg. Sim.), difference between Avg. Obs. and
535 Avg. Sim. (Diff.), root mean square error (RMSE), normalized mean bias (NMB), normalized
536 mean error (NME) and index of agreement (IOA) were calculated to reflect the agreements
537 between the simulated and observed temperature (Temp.), relative humidity (R.H.), wind speed
538 (W.S.), pressure (Press.), NO_2 and O_3, as listed in Table 2. Generally, the lower Diff., RMSE,
539 NMB and NME, but higher IOA indicate better agreement between the simulated and observed
540 values (Willmott et al., 1985). The validation of the simulations of air pollutants was carried out

541 at 8 AQMSs of CNEMC in and around Ji'nan, and at the sampling site, while the meteorological
542 parameters monitored at 6 airports in eastern and northern China and at the sampling site were
543 used to validate the simulated meteorological conditions. The statistics calculated in this study
544 were well within the ranges of those reported in previous studies involving WRF-CMAQ
545 simulations (Table 2) (Jiang et al., 2010; Wang et al., 2015b), suggesting good performance of
546 the model in reproducing the meteorological conditions and air pollutants. Thus, the simulated
547 results were accepted for further analyses.

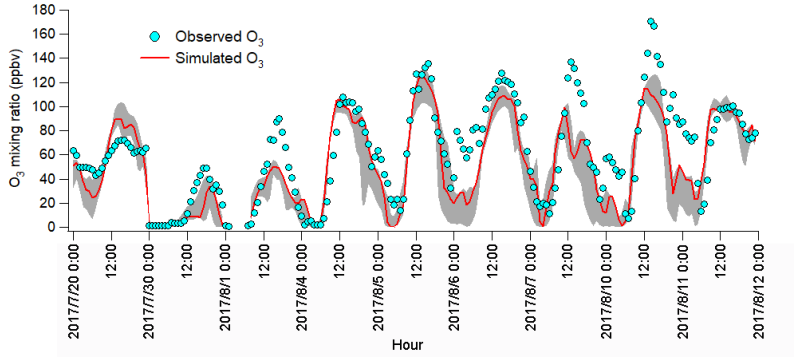

548

549 Figure 5 Hourly average mixing ratios of the WRF-CMAQ simulated and observed O_3 in Ji'nan.
550 The grey area shows the minimum and maximum simulated O_3 at the sampling site and 8
551 adjoining grids (12×12 km^2 for each grid).

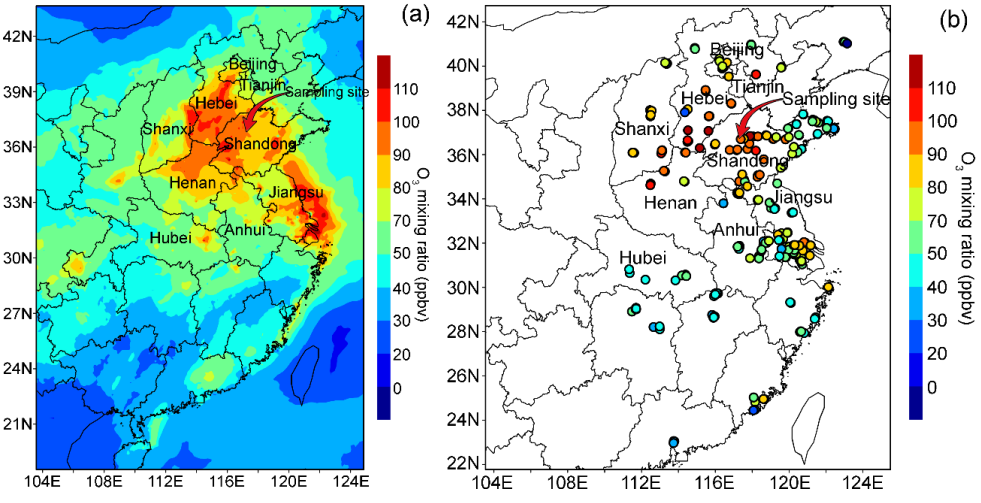

552

553 Figure 6 Comparison between the spatial distributions of (a) the WRF-CMAQ simulated O_3 and
554 (b) the observed O_3 at 14:00 LT averaged over August 4-11. The observed O_3 was acquired from
555 the AQMSs of CNEMC.

556 Table 2 Statistical comparison of the WRF-CMAQ simulated and observed meteorological
557 parameters, O_3 and NO_2. The comparisons were made for the hourly data in 24 hours on all the
558 VOC sampling days.

Meteorological parameter/ Air pollutant	Avg. Obs.	Avg. Sim.	Diff.	RMSE	NMB	NME	IOA
Temp. (℃)	30.0	30.7	0.7	2.4	0.02	0.06	0.89
R.H. (%)	72.7	67.5	-5.2	14.4	-0.06	0.15	0.82
W.S. (m/s)	2.8	3.3	0.5	1.5	0.38	0.56	0.74
Press. (hPa)	1000.5	998.8	-1.7	4.0	-0.002	0.003	0.56
NO_2 (ppbv)	26.7	28.4	1.7	16.7	0.18	0.58	0.73
O_3 (ppbv)	62.8	52.4	-10.4	24.0	-0.07	0.48	0.89

559

560 The IPR analysis quantifies the contributions of different processes to the O_3 production rate, as
561 shown in Figure 7. HDIF and HADV were summed as horizontal transport (HTRA), and the
562 vertical transport (VTRA) was a total representative of VDIF and VADV. It was found that
563 chemical reactions generally led to O_3 decrease during non-episodes. The negative contributions
564 of chemical reactions on July 20 coincided with the very low concentrations of O_3 precursors and
565 the flat diurnal cycle of O_3 (Figure 2). The chemical destruction of O_3 on July 30 and August 1
566 might be related to the relatively weak solar radiation and low temperature, which inhibited the
567 in situ photochemical reactions. In fact, the negative chemical effect should be considered as the
568 titration of NO to regionally-transported and/or background O_3 and the conversion of O_3 to NO_2
569 near NO sources in urban areas (Beck and Grennfelt, 1994; Sillman, 1999). Conversely, the
570 combined effect of horizontal and vertical transport was to increase O_3.

571 During O_3 episodes, chemical reactions made positive contributions to O_3 production between
572 09:00 LT and 15:00 LT, with the average hourly O_3 production rate of 14.0±2.3 ppbv/hr from
573 August 4 to August 11. At the same time, O_3 was also elevated by transport at an average rate of

574 18.7±4.0 ppbv/hr, when the negative effect of vertical transport (-40.8±20.2 ppbv/hr) was
575 reversed by horizontal transport (59.5±19.8 ppbv/hr). The negative contribution of vertical
576 transport to O_3 in these hours might be caused by the updraft with the increase of temperature in
577 the city. The O_3 enhancement by horizontal transport could be explained by the westerly to
578 northerly airflows (Figure 4) and the high O_3 in the areas where the airflows originated or passed
579 (Figure 6). Note that O_3 transported to Ji'nan was still from the NCP, hence we concluded that
580 the NCP was an O_3 source in this case. In fact, the transport of air pollutants (including O_3) from
581 the lower troposphere over the NCP to the free troposphere and further to northeast China was
582 previously identified by Ding et al. (2009), who suggested that the pollutants could be even
583 transported to North America and the Arctic.

584 During 16:00-08:00 LT on O_3 episode days, O_3 was titrated and chemically consumed at the rate
585 of 49.4±6.3 ppbv/hr. This was reasonable in view of the fresh vehicular emissions (particularly
586 NO_x) in the morning and evening rush hours, when the titration of O_3 by NO produced NO_2. The
587 NO_2 was carried over to the other places by air circulation, and/or oxidized to NO_3 and N_2O_5,
588 which could further react with aerosol to form HNO_3 and $ClNO_2$ in the evening. Horizontal and
589 vertical transport dominated O_3 sources, with the average positive contribution of 5.7±7.0 and
590 54.5±9.6 ppbv/hr during 16:00-08:00 LT on August 4-11, respectively. The strong vertical
591 transport coincided with the downward winds in the evening, which might bring the high-altitude
592 O_3 to the ground, as indicated by Figure S9. However, the sources of O_3 in the upper atmosphere
593 were beyond the scope of this study.

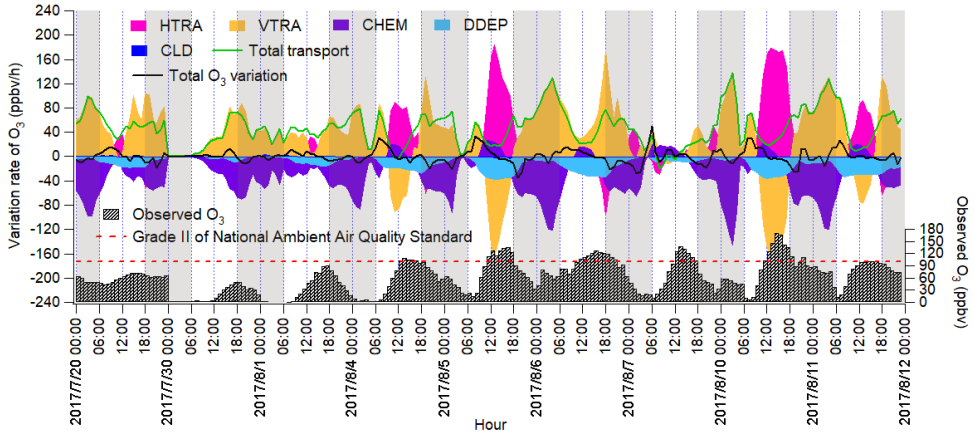

594

595 Figure 7 Time series of O_3 variation rate in Ji'nan induced by individual processes calculated
596 based on the change of O_3 per hour. Total transport is the sum of HTRA and VTRA, and the sum
597 of O_3 variation rates attributable to all the processes is represented by total O_3 variation rate. The
598 nighttime (18:00 – 06:00 LT) has been highlighted in grey.

599 **3.4 Local O_3 formation and control**

600 **3.4.1 Pathway and source contributions to O_3 production**

601 Figure 8 shows the profiles of the six sources of O_3 precursors extracted from PMF. The first
602 source contained high levels of *n*/*i*-pentanes and aromatics, likely representing gasoline exhaust
603 (Ho et al., 2009; Ling and Guo, 2014). The heavy (C_8-C_{10}) hydrocarbons dominated in the
604 second source accompanied by great abundances of the combustion tracers, such as C_2-C_3
605 hydrocarbons, CO, NO and NO_2, in line with the features of diesel exhaust (Liu et al., 2008). The
606 third source was assigned as BVOC, due to the exclusively high loading of isoprene (Guenther,
607 2006). The fourth source was rich in C_4 hydrocarbons, including *n*/*i*-butanes and 1,3-butadiene.
608 It was defined as liquefied petroleum gas (LPG) usage, since butanes and butenes are present in
609 large quantities in China's LPG (Song et al., 2008 and references therein). Solvent usage was
610 represented by the fifth source, in view of the high loadings of hexane isomers (2,3-
611 dimethylbutane, 2-methylpentane and 3-methylpentane) and moderate loadings of *n*-hexane,
612 toluene, ethylbenzene and xylenes (Guo et al., 2011). At last, most of styrene, benzene, toluene,
613 exthylbenzene and xylenes are allocated to the sixth source, which also contained moderate
614 levels of light (C_2-C_5) hydrocarbons. Since styrene is a common petrochemical product (Jobson
615 et al., 2004; Liu et al., 2008), this source was designated as petrochemical industry.

Atmos. Chem. Phys. Discuss., https://doi.org/10.5194/acp-2018-970
Manuscript under review for journal Atmos. Chem. Phys.
Discussion started: 27 September 2018

Atmospheric Chemistry and Physics Discussions

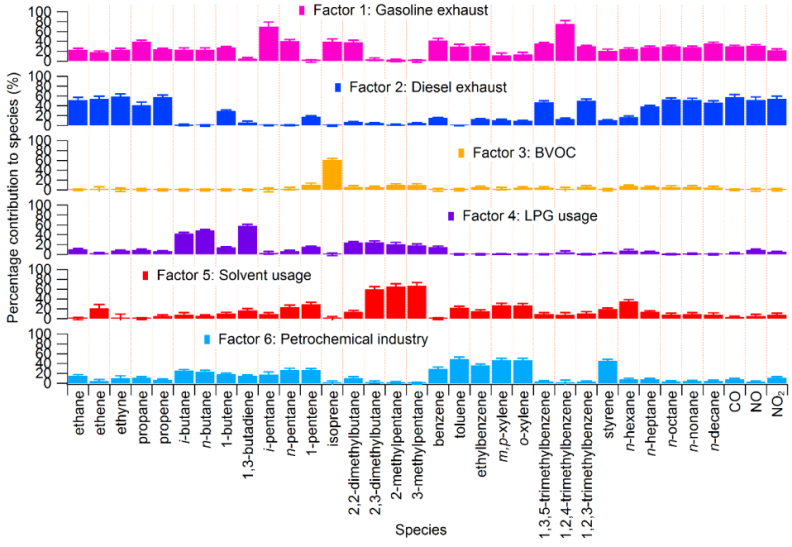

Figure 8 Profiles of the six sources of O_3 precursors in daytime of the VOC sampling days in Ji'nan.

Table 3 summarizes the percentage contributions of specific sources to O_3 precursors. Around a quarter (25.7±3.6%, referring to VOC mixing ratios and hereafter) of VOCs* was attributable to gasoline exhaust. Diesel exhaust, LPG usage, solvent usage and petrochemical industry made comparable (p>0.05) contributions to VOCs*, ranging from 14.7±2.0% to 18.8±3.1%. BVOC constituted the smallest part of VOCs*, accounting for 6.1±2.6%. Most (80-90%) of CO, NO and NO_2 were assigned to the exhausts from diesel and gasoline vehicles, particularly to diesel exhaust which was responsible for more than half of these trace gases.

Table 3 Contributions to VOCs, CO, NO, NO_2 and O_3 production rate by the sources of O_3 precursors averaged on the VOC sampling days in Ji'nan (Unit: % unless otherwise specified).

Source	VOCs*	CO	NO	NO_2	O_3 production rate (ppbv/hr)	
					O_3 episodes	Non-episodes
GE [1]	25.7±3.6	29.9±2.1	30.9±2.4	22.2±2.4	1.8±0.6	1.0±0.3
DE [2]	17.6±2.4	57.3±5.2	52.0±5.8	54.4±5.8	1.7±0.4	1.0±0.3
BVOC	6.1±2.6	0.0±1.7	0.0±2.8	0.0±2.3	1.2±0.5	0.2±0.1
LPG [3]	14.7±2.0	2.2±1.1	9.1±1.6	4.7±0.9	0.8±0.5	0.1±0.1
Solvent [4]	17.1±3.9	3.1±1.8	5.1±3.8	7.8±3.1	0.8±0.5	0.7±0.3

PI [5]	18.8±3.1	7.4±1.9	2.9±1.8	10.9±2.5	1.0±0.3	-0.1±0.1

[1] gasoline exhaust, [2] diesel exhaust, [3] LPG usage, [4] solvent usage and [5] petrochemical industry.

According to the process analysis by WRF-CMAQ, local photochemical formation was an important source of O_3 on episode days in Ji'nan, particularly during 09:00-15:00 LT when O_3 was at high levels (Figure 7). To investigate the local O_3 formation mechanisms, the PBM-MCM model was used to simulate the contributions of pathways and O_3 precursor sources to O_3 production. Table S4 lists the production and destruction pathways of O_3, which have been widely adopted in previous studies (Thornton et al., 2002; Monks, 2005; Kanaya et al., 2009). Briefly, the oxidation of NO by HO_2 and RO_2 produced NO_2, which led to O_3 formation following NO_2 photolysis (R2 and R4-R5 in introduction). Therefore, the reactions between NO and HO_2/RO_2 were considered as the production pathways of O_3. To account for O_3 destruction, reaction between $O^1(D)$ and H_2O denoted the photolysis of O_3, and reactions of O_3 with OH, HO_2 and alkenes were also included. Furthermore, since the formation of HNO_3 through reaction of OH and NO_2 served as an important removal of NO_2, in addition to NO_2 photolysis which produced O_3 eventually, reaction between OH and NO_2 was treated to be destructive to O_3. The titration of O_3 by NO was not treated as an O_3 destruction pathway, because it produced NO_2 with the same amount of O_3 consumed. Though a fraction of NO_2 generated from the titration reaction could be removed by OH, leading to a net destruction of O_3 by NO titration, this was considered in the reaction between NO_2 and OH.

Figure 9 (a) and (b) show the 24 hour average simulated pathway contributions to O_3 production rate for the 6 O_3 episode days and 3 non-episode days. Also shown are the O_3 production rates simulated by PBM-MCM (O_3 production $_{\text{PBM-MCM}}$), those explained by chemical reactions extracted from WRF-CMAQ simulation (O_3 production $_{\text{CHEM in WRF-CMAQ}}$), and those calculated from the observed hourly O_3 (O_3 production $_{\text{obs.}}$). Overall, O_3 production$_{\text{PBM-MCM}}$ and O_3 production $_{\text{obs.}}$ had the same magnitudes, especially during O_3 episodes with more stagnant weather conditions (section 3.2). This indicated that the PBM-MCM model reasonably reproduced the in situ O_3 photochemistry. O_3 production$_{\text{CHEM in WRF-CMAQ}}$ was generally lower than O_3 production$_{\text{PBM-MCM}}$ and O_3 production $_{\text{obs}}$. However, the chemical O_3 productions simulated by WRF-CMAQ and PBM-MCM agreed well with each other during 10:00-15:00 LT on episode days, which might be explained by the dominant role of CHEM in O_3 sources in this period

(Figure 7). The lower or even negative chemical contributions to O_3 productions simulated by WRF-CMAQ resulted from the titration of the regionally transported and/or local background O_3 by NO and the following depletion of NO_2 through reacting with OH and/or transport. Differently, PBM-MCM did not consider the transport of O_3, though the transport effect was partially represented by constraining the model to the observed concentrations of O_3 precursors. In addition, in contrast to the emission-based models (*e.g.*, WRF-CMAQ), PBM-MCM was constructed by the observed air pollutants, which were already subject to chemical reactions before being detected by the analytical instruments. This meant that the reaction between NO and O_3 from the emission to the detection of NO_x was not considered in PBM-MCM. However, as an emission-based model, WRF-CMAQ might perform better in describing the reactions immediately after the emissions of air pollutants. Therefore, the chemical destructions of O_3 in the vicinity of NO_x sources might also account for the aforementioned discrepancy. The obviously higher reaction rate between NO and O_3 simulated by WRF-CMAQ (Figure S11) confirmed our inferences.

During both O_3 episodes and non-episodes, the reaction between HO_2 and NO dominated over "RO_2+NO" in O_3 production, while the O_3 destruction was mainly attributable to the formation of HNO_3 ($OH+NO_2 \rightarrow HNO_3$), the reaction between O_3 and HO_2 and photolysis of O_3, *i.e.* $O^1(D)+H_2O$. Note that the formation of nitric acid did not directly destroy O_3, but consumed NO_2 and consequently reduced O_3 production rate. The net O_3 production rate during O_3 episodes (maximum: 21.3 ppbv/hr) was much ($p<0.05$) higher than during non-episodes (maximum: 16.9 ppbv/hr), which partially explained the higher O_3 on episode days. In general, "$OH+NO_2$" serves as the chain terminating reaction in VOC-limited regime of O_3 formation, while the radical-radical reactions take over the role in NO_x-limited regime (Finlayson-Pitts and Pitts, 1993; Kleinman, 2005). Here, we found that the ratio of total reaction rates between "HO_2+RO_2" and "$OH+NO_2$" substantially increased from 0.2 ± 0.1 during non-episodes to 1.0 ± 0.3 during O_3 episodes ($p<0.05$). This suggested that O_3 formation during non-episodes was limited by VOCs, while it might switch to be co-limited by VOCs and NO_x during episodes in view of the equivalent role of "HO_2+RO_2" and "$OH+NO_2$" in terminating the chain reactions.

Further, the 24 hour average contributions to net O_3 production rate of different sources of O_3 precursors were identified for the 6 episode days and 3 non-episode days, as presented in Figure

687 9 (c) and (d). The source contributions to the O_3 production rate were obtained from the
688 differences in simulated O_3 production rates between a base run and a constrained run. In the
689 base run, the O_3 production rate was simulated with the observed concentrations of air pollutants
690 except for the carbonyls, while the concentrations of air pollutants attributable to a specific
691 source were deducted from the observed concentrations in the input of the constrained run. To
692 account for the influence of primary hydrocarbons on the formation of carbonyls, and the
693 subsequent impact on O_3 production, carbonyls were not constrained to observations in either the
694 base run or the constrained runs. However, the source-specific primary emissions of carbonyls
695 and their contributions to O_3 production were not considered in this approach. Therefore, the
696 source-specific contributions to net O_3 production rate were expected to be underestimated, as
697 carbonyls are generally of high O_3 formation potentials (Cheng et al., 2010; Dong et al., 2014).
698 The method was applied to each of the six sources, derived from the PMF analysis, thereby
699 acquiring the contribution to O_3 production rate of each source.

700 On average, the source contributions (in ppbv/hr) to O_3 production rates during O_3 episodes and
701 non-episodes are presented in Table 3. It was found that gasoline exhaust and diesel exhaust
702 were the largest contributors to O_3 production regardless of O_3 episodes or non-episodes.
703 Specifically, the net O_3 production rate was 1.0±0.3 ppbv/hr for both gasoline and diesel exhaust
704 during non-episodes, which however increased to 1.8±0.6 ppbv/hr for gasoline exhaust and
705 1.7±0.4 ppbv/hr for diesel exhaust during O_3 episodes. This suggested that vehicular emissions
706 played critical roles in building up ground-level O_3 in Ji'nan. If carbonyls were taken into
707 account, the contributions of vehicular emissions to O_3 production rate were even higher than the
708 currently simulated values, due to the dominance of vehicular exhausts in the sources of
709 carbonyls in urban areas (Grosjean et al., 1990; Granby et al., 1997). In addition, the
710 contributions of the other sources to O_3 production rates all increased during O_3 episodes except
711 for solvent usage (p>0.05), as listed in Table 3. It is not surprising to see the coincident increases,
712 in view of the higher simulated and observed overall O_3 production rate during episodes. Further
713 insight into the percentage contributions (not shown here) found that the contributions of BVOC,
714 LPG usage and petrochemical industry relative to the sum of the O_3 production rates of the 6
715 sources increased substantially from 9.9±4.2%, 4.3±1.4% and -2.8±1.9% during non-episodes to
716 19.2±4.3%, 9.1±3.4% and 12.1±3.1% during O_3 episodes, respectively. The increased O_3
717 production rates by BVOCs could be explained by the increase of isoprene (episodes: 2.2±0.6

718 ppbv; non-episodes: 0.9±0.3 ppbv), under higher temperature and stronger solar radiation during
719 O_3 episodes. The enhanced O_3 formation from petrochemical industry on episode days was likely
720 associated with the dominance of continental air (Figure 4) and the extensive petrochemical
721 industries in the NCP, elevating the concentrations of photochemical VOCs. For example, the
722 observed mixing ratio of styrene increased from 54.7±22.0 pptv during non-episodes to
723 162.3±44.7 pptv during O_3 episodes. The reason for elevated O_3 production rate by LPG usage
724 during episodes was unknown. It is worth noting that the source contributions to O_3 production
725 might have some uncertainty due to the limited number of samples (54 samples) and O_3
726 precursors (31 VOCs, CO, NO and NO_2) for source apportionment.

727

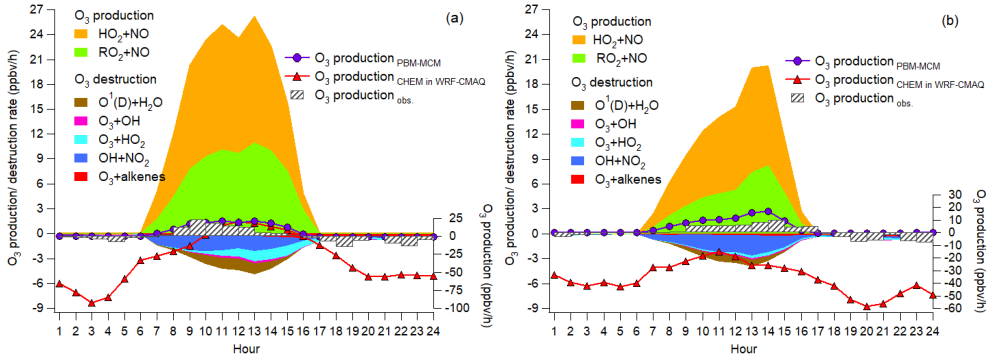

728

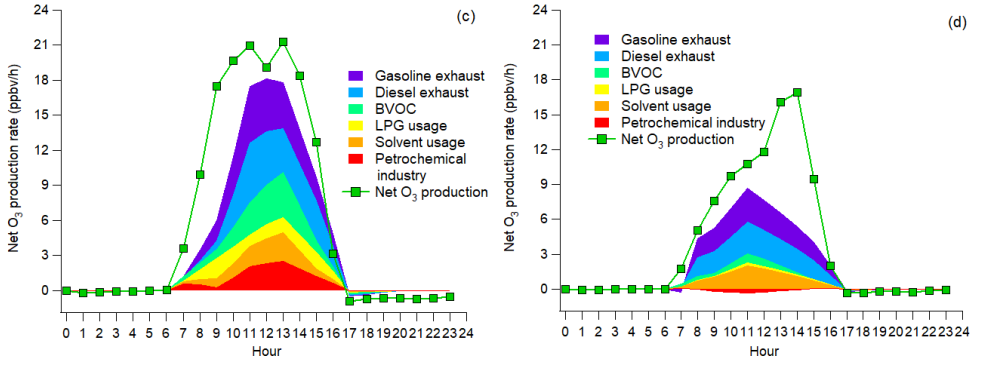

729 Figure 9 Pathway contributions to O_3 production and destruction rate during episodes (a) and
730 non-episodes (b). Contributions of O_3 precursor sources to net O_3 production rate during
731 episodes (c) and non-episodes (d).

732 **3.4.2 O_3 control measures**

As the tropospheric O_3 is produced through the reactions between VOCs and NO_x, the relationships between O_3 and the precursors were investigated. Since WRF-CMAQ simulated the highest contribution of chemical reactions to O_3 production rate at 9:00-15:00 LT and the PBM-MCM indicated the maximum O_3 production rate at 12:00 LT, the isopleths of the net O_3 production rate at 12:00 LT are plotted in Figure 10, as a function of the OH reactivity of VOCs ($OH\ reactivity_{VOCs}$) and NO_x ($OH\ reactivity_{NOx}$). The OH reactivity instead of the absolute concentrations was plotted, because we intended to show the reactivity-dependent reductions of source emissions, as discussed later. It is noteworthy that the OH reactivity was calculated as the products of the observed concentrations of O_3 precursors and the corresponding reaction rate constants between O_3 precursors and OH, rather than observed or modeled values. $OH\ reactivity_{VOCs}$ in Figure 10 are the percentages relative to the average $OH\ reactivity_{VOCs}$ during O_3 episodes of the VOC sampling days, the same for $OH\ reactivity_{NOx}$. The scenario with both $OH\ reactivity_{VOCs}$ and $OH\ reactivity_{NOx}$ equaling 100% represents the average $OH\ reactivity_{VOCs}$ and $OH\ reactivity_{NOx}$ during O_3 episodes, respectively. The $OH\ reactivity_{VOCs}$ throughout the VOC sampling period were within the range of 33-123% of the average $OH\ reactivity_{VOCs}$ during O_3 episodes. For $OH\ reactivity_{NOx}$, the range was 61-242%. To include the OH reactivity of VOCs and NO_x on all the VOC sampling days, factors from 10% to 140% with the step of 10% were applied to the average diurnal profiles of VOCs and CO during O_3 episodes, while the factors ranged from 10% to 300% with the step of 10% for NO_x. For example, when the average VOCs and NO_x during O_3 episodes were multiplied by a factor of 50% and 120%, respectively, $OH\ reactivity_{VOCs}$ and $OH\ reactivity_{NOx}$ in this scenario were 50% and 120% of those averaged over O_3 episodes, respectively. The initial concentrations of all air pollutants were also scaled by these same factors and the model was constrained to these scaled concentrations every hour, except for O_3, which was not a model input. It should be noted that the factors applied to CO were exactly the same as those applied to VOCs, therefore we use $VOCs^{\#}$ to represent the sum of VOCs and CO hereafter. The 14 gradients of $OH\ reactivity_{VOCs^{\#}}$ and 30 gradients of $OH\ reactivity_{NOx}$ made up 420 scenarios, thus the isopleths were made with 420 simulated O_3 production rates at 12:00 LT. Meteorological conditions were exactly the same for all the scenarios and the clear sky was hypothesized.

As shown in Figure 10, O_3 formation can be divided into $VOC^{\#}$-limited regime and NO_x-limited regime with the method used in Lyu et al. (2017). Briefly, at a given $OH\ reactivity_{VOCs^{\#}}$, O_3 production rate generally reached the maximum at a specific $OH\ reactivity_{NOx}$ due to the dual role of NO_x in O_3 formation. The scenario with this specific $OH\ reactivity_{NOx}$ was treated as dividing point between NO_x-limited regime and $VOC^{\#}$-limited regime. Since 14 gradients of $OH\ reactivity_{VOCs^{\#}}$ (10% - 140% with the step of 10%) were set for all the scenarios, 14 pairs of $OH\ reactivity_{NOx}$ and $OH\ reactivity_{VOCs^{\#}}$ were obtained, as shown by the orange crosses in Figure 10. A dividing line was acquired from the linear regression between $OH\ reactivity_{VOCs^{\#}}$ and $OH\ reactivity_{NOx}$ in these scenarios (orange dashed line in Figure 10). O_3 formation was limited by $VOCs^{\#}$ and NO_x in the lower right and upper left of the dividing line, respectively. Since the horizontal and vertical coordinates were percentages relative to the average $OH\ reactivity_{VOCs^{\#}}$ and $OH\ reactivity_{NOx}$ during O_3 episodes, rather than the actual values of OH reactivity, we did not present the dividing ratio of $\frac{OH\ reactivity_{VOCs^{\#}}}{OH\ reactivity_{NOx}}$ here. Further, it was found that O_3 production rate was also enhanced with the increase of $OH\ reactivity_{VOCs^{\#}}$ in the upper left area close to the dividing line. We defined it as a transition area where the O_3 production rate was comparably sensitive to $VOCs^{\#}$ and NO_x. Beyond the transition area in the upper left of the dividing line, the sensitivity of O_3 production rate to NO_x was generally ten times higher than to $VOCs^{\#}$, which was designated as NO_x-limited regime. The transition area and the NO_x-limited regime are divided by the blue dashed line in Figure 10.

Based on these sensitivity simulations, it was found that O_3 formation was mainly limited by $VOCs^{\#}$ during non-episodes. However, it switched to be co-limited by $VOCs^{\#}$ and NO_x (transition regime) on episode days with the net O_3 production rate among the highest, except for August 5 when the strong sea breeze might dilute air pollutants in Ji'nan and/or intercept the transport of air pollutants from Central China to Ji'nan (Figure S6). Theoretically, it was also possible that O_3 formation was limited by NO_x during episodes, in view of the overestimation of NO_2 by the chemiluminescence analyzer which was expected to be more significant than during non-episodes. However, O_3 formation was not likely only limited by NO_x, which should be still sensitive to VOCs, as NO_2 could not be much overestimated in the urban areas (see section 2.2.1). Therefore, O_3 formation was considered to be in the transition regime during episodes. This might partially explain the increased O_3 during episodes in Ji'nan, given the higher O_3

production rates in transition area (Figure 10). Noticeably, this trend is also consistent with the regime change predicted by the $\frac{OH\ reactivity_{VOCs^{\#}}}{OH\ reactivity_{NOx}}$ presented in section 3.1.

Furthermore, since O_3 formation during episodes was generally co-limited by VOCs$^{\#}$ and NO_x or even more limited by NO_x considering the overestimation of NO_2, it was expected that reducing emissions of either VOCs$^{\#}$ or NO_x would alleviate O_3 pollution on high O_3 days. However, the decrease of NO_x would enhance O_3 production during non-episodes. This meant that a compromise should be made between the reduction of average O_3 (during non-episodes) and highest O_3 (during episodes) when the O_3 control measures mainly focused on NO_x in Ji'nan. The effects of emission restrictions of O_3 precursors from specific sources, as indicated by PMF analysis, on $OH\ reactivity_{VOCs^{\#}}$ and $OH\ reactivity_{NOx}$ are presented in Figure 10 (straight solid lines #1-#6). The start point of the straight lines corresponded to 100% of $OH\ reactivity_{VOCs^{\#}}$ and $OH\ reactivity_{NOx}$, namely the average condition during O_3 episodes. The end points, however, denote $OH\ reactivity_{VOCs^{\#}}$ and $OH\ reactivity_{NOx}$ in the atmosphere when the specific source emissions are removed. Therefore, the length of the lines reflects the potential of each PMF-derived O_3 precursor source to alter $OH\ reactivity_{VOCs^{\#}}$ and $OH\ reactivity_{NOx}$ in the atmosphere. Clearly, diesel and gasoline exhausts were the sources significantly contributing to the $OH\ reactivity_{VOCs^{\#}}$ and $OH\ reactivity_{NOx}$ during O_3 episodes. Emission restriction of vehicle exhausts during O_3 episodes would greatly benefit O_3 reduction in Ji'nan. Figure S12 shows the simulated O_3 production rate as a function of the source emission reduction, which also confirmed the highest efficiencies of O_3 reduction by cutting diesel exhaust (0.58 ppbv h^{-1}/10% emission reduction) and gasoline exhaust (0.47 ppbv h^{-1}/10% emission reduction). We also found that the reduction of diesel exhaust would lead to the increase of O_3 production rate when the reduction percentages were lower than a dividing point (*e.g.*, 60% on August 10), while further reductions would decrease the O_3 production rate. This was due to high emission of NO_x from diesel vehicles and dual roles of NO_x in O_3 formation. However, the enhancement of O_3 production rate was very minor (<0.1 ppbv/hr), as the O_3 formation during episodes was in the transition area. In fact, constraint on diesel exhaust would progressively shift O_3 formation to a NO_x-limited regime where cutting NO_x would be quite effective for O_3 control (red line in Figure 10). Therefore, constraints of vehicle emissions are most effective on O_3 abatement in Ji'nan. It is noteworthy that VOCs$^{\#}$ and NO_x (if any) in all the sources were cut in

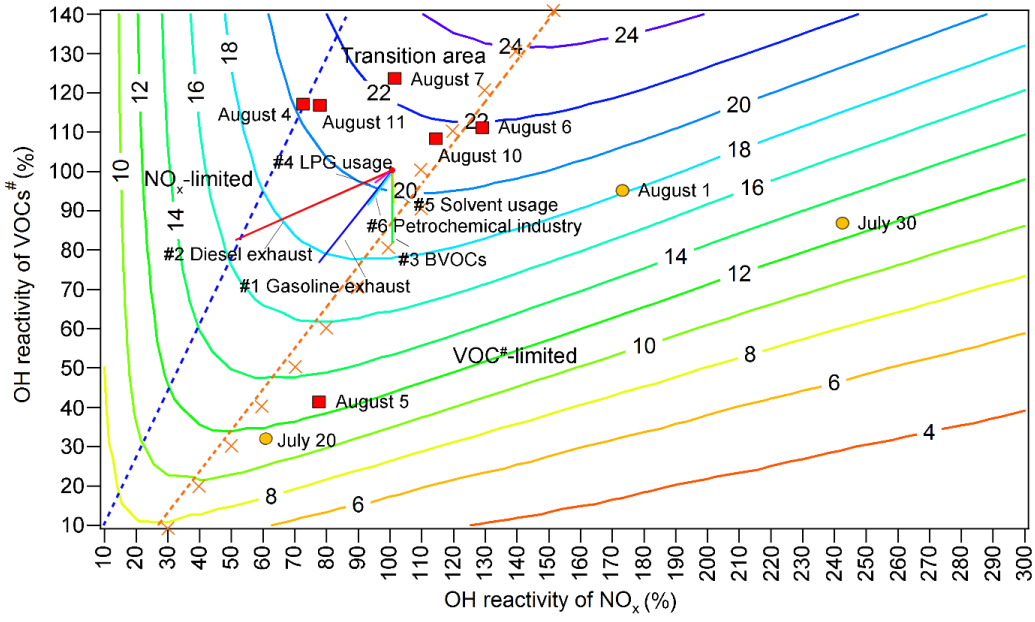

Figure 10 Isopleths of the net O_3 production rate (ppbv/hr) at 12:00 LT as a function of $OH\ reactivity_{VOCs^{\#}}$ and $OH\ reactivity_{NOx}$. The red blocks and orange circles denote the calculated $OH\ reactivity_{VOCs^{\#}}$ and $OH\ reactivity_{NOx}$ at 12:00 LT on O_3 episode and non-episode days, respectively. Each orange cross represents the $OH\ reactivity_{VOCs^{\#}}$ and $OH\ reactivity_{NOx}$ at 12:00 LT in the scenario with highest O_3 production rate at a given $OH\ reactivity_{VOCs^{\#}}$. The orange dashed line and blue dashed line divide O_3 formation into the VOC-limited regime, transition area, and NO_x-limited regime.

4 Implications

This study investigates the causes of a severe O_3 pollution event lasting for eight consecutive days in the NCP, one of the most densely populated regions in the world. Photochemical O_3 formation in the lower troposphere of the NCP is demonstrated as the main source, under the synoptic conditions of weak high pressure or low pressure trough. Though NO_x, as an important precursor of O_3, has been significantly reduced in emissions in China since 2011 (Duncan et al., 2016; Liu et al., 2017), O_3 pollution is still severe or even becoming worse in the NCP, as

revealed in the present and also previous studies (Zhang et al., 2014; Sun et al., 2016). The finding that O_3 formation shifted from VOC-limited regime on relatively low O_3 days to the transition area on O_3-unattainment days may elucidate the cause of the increase in O_3, because O_3 productions in the transition area are even higher, despite decreases in NO_x emissions. Consistent with previous studies, the NCP is identified as a source region of O_3 in this study. It can be expected that organic nitrates are also intensively formed as byproducts in the photochemical cycles of O_3 formation. In combination with the fact that the NCP locates within the mid-latitude band of Northern Hemisphere under the dominance of westerlies, O_3 and organic nitrates formed in this region can be transported over a long distance following uplift processes, which has been confirmed to partially account for the enhancement of background O_3 in North America and even Europe (Derwent et al., 2015; Lin et al., 2017). Taking into consideration the high O_3 levels and their upward trend in the NCP, it is not realistic to believe that the reduction of NO_x in China will ease the global O_3 burden in a short period. More stringent control measures may be needed to achieve an O_3 benefit, with comprehensive thinking of atmospheric dynamics and chemistry.

Acknowledgements: This study was supported by the National Key R&D Program of China (2017YFC0212001), the Research Grants Council of the Hong Kong Special Administrative Region via grants PolyU5154/13E, PolyU152052/14E, PolyU152052/16E, CRF/C5004-15E and CRF/C5022-14G, the Collaborative Research program between The Beijing University of Technology and The Hong Kong Polytechnic University (PolyU) (4-ZZFW), the Hong Kong Polytechnic University PhD scholarships (project RTUP), and the National Natural Science Foundation of China (No. 41675118). This study is partly supported by the Hong Kong PolyU internal grant (G-YBUQ, 1-ZVJT and 1-BBW4). The data are accessible at https://drive.google.com/open?id=1_KeOxOuVsLY83xL74RtcRORsiiyIR 8FZ.

References

Atkinson, R.: Atmospheric chemistry of VOCs and NO_x, Atmos. Environ., 34, 2063-2101, **2000**.

Beck, J.P. and Grennfelt, P.: Estimate of ozone production and destruction over northwestern Europe, Atmos. Environ., 28, 129-140, **1994**.

868 Cai, C., Geng, F., Tie, X., Yu, Q., and An, J.: Characteristics and source apportionment of VOCs
869 measured in Shanghai, China, Atmos. Environ., 44, 5005-5014, **2010**.

870 Carter, W. P.: Development of ozone reactivity scales for volatile organic compounds, Air &
871 Waste Manage. Assoc., 44, 881-899, **1994**.

872 Carter, W. P., Pierce, J. A., Luo, D., and Malkina, I. L.: Environmental chamber study of
873 maximum incremental reactivities of volatile organic compounds, Atmos. Environ., 29(18),
874 2499-2511, **1995**.

875 Chameides, W. and Walker, J.C.: A photochemical theory of tropospheric ozone, J. Geophys.
876 Res., 78(36), 8751-8760, **1973**.

877 Chan, C. Y. and Chan, L. Y.: Effect of meteorology and air pollutant transport on ozone episodes
878 at a subtropical coastal Asian city, Hong Kong, J. Geophys. Res. - atmospheres, 105(D16),
879 20707-20724, **2000**.

880 Chen, Y., Zhao, C., Zhang, Q., Deng, Z., Huang, M., and Ma, X.: Aircraft study of mountain
881 chimney effect of Beijing, China, J. Geophys. Res. - Atmospheres, 114(D8),
882 doi:10.1029/2008JD010610, **2009**.

883 Cheng, H., Guo, H., Wang, X., Saunders, S. M., Lam, S. H. M., Jiang, F., Wang, T., Ding, A.,
884 Lee, S., and Ho, K. F.: On the relationship between ozone and its precursors in the Pearl River
885 Delta: application of an observation-based model (OBM), Environ. Sci. Pollut. Res., 17(3), 547-
886 560, **2010**.

887 Colman, J. J., Swanson, A. L., Meinardi, S., Sive, B. C., Blake, D. R., and Rowland, F. S.:
888 Description of the analysis of a wide range of volatile organic compounds in whole air samples
889 collected during PEM-Tropics A and B, Anal. Chem., 73(15), 3723-3731, **2001**.

890 Crutzen, P.: A discussion of the chemistry of some minor constituents in the stratosphere and
891 troposphere, Pure & Applied Geophysics, 106(1), 1385-1399, **1973**.

892 Derwent, R.G., Utembe, S.R., Jenkin, M.E., Shallcross, D.E., 2015. Tropospheric ozone
893 production regions and the intercontinental origins of surface ozone over Europe. Atmospheric
894 Environment, 112, 216-224.

895 Dong, D., Shao, M., Li, Y., Lu, S., Wang, Y., Ji, Z., and Tang, D.: Carbonyl emissions from
896 heavy-duty diesel vehicle exhaust in China and the contribution to ozone formation potential, J.
897 Environ. Sci., 26(1), 122-128, **2014**.

898 Duncan, B.N., Lamsal, L.N., Thompson, A.M., Yoshida, Y., Lu, Z., Streets, D.G., Hurwitz,
899 M.M., Pickering, K.E., 2016. A space-based, high-resolution view of notable changes in urban
900 NO_x pollution around the world (2005-2014). Journal of Geophysical Research: Atmospheres,
901 121(2), 976-996.

902 Dunlea, E.J., Herndon, S.C., Nelson, D.D., Volkamer, R.M., San Martini, F., Sheehy, P.M.,
903 Zahniser, M.S., Shorter, J.H., Wormhoudt, J.C., Lamb, B.K., and Allwine, E.J.: Evaluation of
904 nitrogen dioxide chemiluminescence monitors in a polluted urban environment, Atmos. Chem.
905 Phys., 7(10), 2691-2704, **2007**.

906 Finlayson-Pitts, B.J., and Pitts Jr, J.N.: Atmospheric chemistry of tropospheric ozone formation:
907 scientific and regulatory implications, Air & Waste Manage. Assoc., 43(8), 1091-1100, **1993**.

908 Fung, J. C. H., Lau, A. K. H., Lam, J. S. L., and Yuan, Z.: Observational and modeling analysis
909 of a severe air pollution episode in western Hong Kong, J. Geophys. Res. - Atmospheres,
910 110(D9), **2005**.

911 Gao, J., Wang, T., Ding, A., and Liu, C.: Observational study of ozone and carbon monoxide at
912 the summit of mount Tai (1534m asl) in central-eastern China, Atmos. Environ., 39(26), 4779-
913 4791, **2005**.

914 Granby, K., Christensen, C.S., and Lohse, C.: Urban and semi-rural observations of carboxylic
915 acids and carbonyls, Atmos. Environ., 31(10), 1403-1415, **1997**.

916 Grosjean, D., Miguel, A.H., and Tavares, T.M.: Urban air pollution in Brazil: Acetaldehyde and
917 other carbonyls, Atmos. Environ.: Part B. Urban Atmosphere, 24(1), 101-106, **1990**.

918 Guenther, A., Karl, T., Harley, P., Wiedinmyer, C., Palmer, P.I., and Geron, C.: Estimates of
919 global terrestrial isoprene emissions using MEGAN (Model of Emissions of Gases and Aerosols
920 from Nature), Atmos. Chem. Phys., 6(11), 3181-3210, **2006**.

921 Guo, H., Cheng, H.R., Ling, Z.H., Louie, P.K., and Ayoko, G.A.: Which emission sources are
922 responsible for the volatile organic compounds in the atmosphere of Pearl River Delta? J. Hazard.
923 Mat., 188(1-3), 116-124, **2011**.

924 Guo, H., Ling, Z. H., Cheung, K., Jiang, F., Wang, D. W., Simpson, I. J., Barletta, B., Meinardi,
925 S., Wang, T. J., Wang, X. M., Saunders, S. M., and Blake, D. R.: Characterization of
926 photochemical pollution at different elevations in mountainous areas in Hong Kong, Atmos.
927 Chem. Phys., 13(8), 3881-3898, **2013**.

928 He, J., Wang, Y., Hao, J., Shen, L., and Wang, L.: Variations of surface O_3 in August at a rural
929 site near Shanghai: influences from the West Pacific subtropical high and anthropogenic
930 emissions, Environ. Sci. Pollut. Res., 19(9), 4016-4029, **2012**.

931 He, K.: Multi-resolution Emission Inventory for China (MEIC): model framework and 1990-
932 2010 anthropogenic emissions, In AGU Fall Meeting Abstracts, December, **2012**.

933 Ho, K.F., Lee, S.C., Ho, W.K., Blake, D.R., Cheng, Y., Li, Y.S., Ho, S.S., Fung, K., Louie, P.K.,
934 and Park, D.: Vehicular emission of volatile organic compounds (VOCs) from a tunnel study in
935 Hong Kong, Atmos. Chem. Phys., 9(19), 7491-7504, **2009**.

936 Hu, J., Chen, J., Ying, Q., and Zhang, H.: One-year simulation of ozone and particulate matter in
937 China using WRF/CMAQ modeling system, Atmos. Chem. Phys., 16(16), 10333–10350, **2016**.

938 Huang, J. P., Fung, J. C., Lau, A. K., and Qin, Y.: Numerical simulation and process analysis of
939 typhoon-related ozone episodes in Hong Kong, J. Geophys. Res. - Atmospheres, 110(D5), **2005**.

940 Jenkin, M.E. and Clemitshaw, K.C.: Ozone and other secondary photochemical pollutants:
941 chemical processes governing their formation in the planetary boundary layer, Atmos. Environ.,
942 34(16), 2499-2527, **2000**.

943 Jenkin, M.E., Saunders, S.M., and Pilling, M.J.: The tropospheric degradation of volatile organic
944 compounds: a protocol for mechanism development, Atmos. Environ., 31(1), 81-104, **1997**.

945 Jiang, F., Guo, H., Wang, T. J., Cheng, H. R., Wang, X. M., Simpson, I. J., Ding, A. J., Saunders,
946 S. M., Lam, S. H. M., and Blake, D. R.: An ozone episode in the Pearl River Delta: Field
947 observation and model simulation, J. Geophys. Res. - Atmospheres, 115(D22), **2010**.

948 Jobson, B.T., Berkowitz, C.M., Kuster, W.C., Goldan, P.D., Williams, E.J., Fesenfeld, F.C., Apel,
949 E.C., Karl, T., Lonneman, W.A., and Riemer, D.: Hydrocarbon source signatures in Houston,
950 Texas: Influence of the petrochemical industry, J. Geophys. Res. - Atmospheres, 109(D24),
951 doi.org/10.1029/2004JD004887, **2004**.

952 Kanaya, Y., Pochanart, P., Liu, Y., Li, J., Tanimoto, H., Kato, S., Suthawaree, J., Inomata, S.,
953 Taketani, F., Okuzawa, K., and Kawamura, K.: Rates and regimes of photochemical ozone
954 production over Central East China in June 2006: a box model analysis using comprehensive
955 measurements of ozone precursors, Atmos. Chem. Phys., 9(20), 7711-7723, **2009**.

956 Kleinman, L.I.: The dependence of tropospheric ozone production rate on ozone precursors,
957 Atmos. Environ., (3), 575-586, **2005**.

958 Kusaka, H. and Kimura, F.: Coupling a single-layer urban canopy model with a simple
959 atmospheric model: Impact on urban heat island simulation for an idealized case, J. Meteoro. Soc.
960 Japan: Ser. II, 82(1), 67-80, **2004**.

961 Lam, S. H. M., Saunders, S. M., Guo, H., Ling, Z. H., Jiang, F., Wang, X. M., and Wang, T. J.:
962 Modelling VOC source impacts on high ozone episode days observed at a mountain summit in
963 Hong Kong under the influence of mountain-valley breezes, Atmos. Environ., 81, 166-176, **2013**.

964 Lang, J., Zhang, Y., Zhou, Y., Cheng, S., Chen, D., Guo, X., Chen, S., Li, X., Xing, X., and
965 Wang, H.: Trends of $PM_{2.5}$ and chemical composition in Beijing, 2000–2015, Aerosol Air Qual.
966 Res., 17, 412-425, **2017**.

967 Lin, M., Horowitz, L.W., Payton, R., Fiore, A.M., Tonnesen, G., 2017. US surface ozone trends
968 and extremes from 1980 to 2014: quantifying the roles of rising Asian emissions, domestic
969 controls, wildfires, and climate. Atmospheric Chemistry & Physics. 17(4), 2943-2970.

970 Lin, W., Xu, X., Zhang, X., and Tang, J.: Contributions of pollutants from North China Plain to
971 surface ozone at the Shangdianzi GAW Station, Atmos. Chem. Phys., 8(19), 5889-5898, **2008**.

972 Ling, Z. H. and Guo, H.: Contribution of VOC sources to photochemical ozone formation and its
973 control policy implication in Hong Kong, Environ. Sci. Policy, 38, 180-191, **2014**.

974 Liu, F., Beirle, S., Zhang, Q., Zheng, B., Tong, D., He, K., 2017. NO_x emission trends over
975 Chinese cities estimated from OMI observations during 2005 to 2015. Atmospheric chemistry
976 and physics, 17(15), 9261-9275.

977 Liu, X. H., Zhang, Y., Xing, J., Zhang, Q., Wang, K., Streets, D. G., Jang, C., Wang, W. X., and
978 Hao, J. M.: Understanding of regional air pollution over China using CMAQ, part II. Process
979 analysis and sensitivity of ozone and particulate matter to precursor emissions, Atmos. Environ.,
980 44(30), 3719-3727, **2010**.

981 Liu, Y., Shao, M., Fu, L., Lu, S., Zeng, L., and Tang, D.: Source profiles of volatile organic
982 compounds (VOCs) measured in China: Part I, Atmos. Environ., 42(25), 6247-6260, **2008**.

983 Lo, J. C., Lau, A. K., Fung, J. C., and Chen, F.: Investigation of enhanced cross-city transport
984 and trapping of air pollutants by coastal and urban land-sea breeze circulations, J. Geophys. Res.
985 - Atmospheres, 111(D14), **2006**.

986 Lyu, X. P., Guo, H., Wang, N., Simpson, I. J., Cheng, H. R., Zeng, L. W., Saunders, S. M., Lam,
987 S. H. M., Meinardi, S., and Blake, D. R.: Modeling C_1-C_4 alkyl nitrate photochemistry and their
988 impacts on O_3 production in urban and suburban environments of Hong Kong. J. Geophys. Res. -
989 Atmospheres, 122(19), **2017**.

990 Madronich, S. and Flocke, S.: Theoretical estimation of biologically effective UV radiation at the
991 Earth's surface, In Solar Ultraviolet Radiation (pp. 23-48), Springer, Berlin, Heidelberg, **1997**.

992 Mao, J., Ren, X., Chen, S., Brune, W.H., Chen, Z., Martinez, M., Harder, H., Lefer, B.,
993 Rappenglueck, B., Flynn, J., and Leuchner, M.: Atmospheric oxidation capacity in the summer
994 of Houston 2006: Comparison with summer measurements in other metropolitan studies, Atmos.
995 Environ., 44(33), 4107-4115, **2010**.

996 McClenny, W.A., Williams, E.J., Cohen, R.C., and Stutz, J.: Preparing to measure the effects of
997 the NO_x SIP Call—methods for ambient air monitoring of NO, NO_2, NO_y, and individual NO_z
998 species, Air & Waste Manage. Assoc,, 52(5), 542-562, **2002**.

999 McDuffie, E.E., Edwards, P.M., Gilman, J.B., Lerner, B.M., Dube, W.P., Trainer, M., Wolfe,
1000 D.E., Angevine, W.M., deGouw, J., Williams, E.J., and Tevlin, A.G.: Influence of oil and gas

emissions on summertime ozone in the Colorado Northern Front Range, J. Geophys. Res. - Atmospheres, 121(14), 8712-8729, **2016**.

Monks, P. S.: Gas-phase radical chemistry in the troposphere, Chem. Soc. Reviews, 34(5), 376-395, **2005**.

Paatero, P. and Tapper, U.: Positive matrix factorization: A non-negative factor model with optimal utilization of error estimates of data values, Environmetrics, 5(2), 111-126, **1994**.

Ren, X., Harder, H., Martinez, M., Lesher, R.L., Oliger, A., Simpas, J.B., Brune, W.H., Schwab, J.J., Demerjian, K.L., He, Y., and Zhou, X.: OH and HO_2 chemistry in the urban atmosphere of New York City, Atmos. Environ., 37(26), 3639-3651, **2003**.

Saunders, S.M. Jenkin, M.E., Derwent, R.G., and Pilling, M.J.: Protocol for the development of the Master Chemical Mechanism, MCM v3 (Part A): tropospheric degradation of non-aromatic volatile organic compounds, Atmos. Chem. Phys., 3(1), 161-180, **2003**.

Shan, W., Yin, Y., Zhang, J., and Ding, Y.: Observational study of surface ozone at an urban site in East China, Atmos. Res., 89(3), 252-261, **2008**.

Shao, M., Lu, S., Liu, Y., Xie, X., Chang, C., Huang, S., and Chen, Z.: Volatile organic compounds measured in summer in Beijing and their role in ground-level ozone formation, J. Geophys. Res. - Atmospheres, 114(D2), doi.org/10.1029/2008JD010863, **2009b**.

Shao, M., Zhang, Y., Zeng, L., Tang, X., Zhang, J., Zhong, L., and Wang, B.: Ground-level ozone in the Pearl River Delta and the roles of VOC and NOx in its production, J. Environ. Manage., 90(1), 512-518, **2009a**.

Shu, L., Xie, M., Wang, T., Gao, D., Chen, P., Han, Y., Li, S., Zhuang, B., and Li, M.: Integrated studies of a regional ozone pollution synthetically affected by subtropical high and typhoon system in the Yangtze River Delta region, China, Atmos. Chem. Phys., 16(24), 15801-15819, **2016**.

Sillman, S.: The relation between ozone, NO_x and hydrocarbons in urban and polluted rural environments, Atmos. Environ., 33(12), 1821-1845, **1999**.

Sillman, S., Logan, J.A., and Wofsy, S.C.: The sensitivity of ozone to nitrogen oxides and hydrocarbons in regional ozone episodes, J. Geophys. Res. - Atmospheres, 95(D2), 1837-1851, **1990**.

Song, Y., Dai, W., Shao, M., Liu, Y., Lu, S., Kuster, W., and Goldan, P.: Comparison of receptor models for source apportionment of volatile organic compounds in Beijing, China, Environ. Pollut., 156(1), 174-183, **2008**.

Sun, L., Xue, L., Wang, T., Gao, J., Ding, A., Cooper, O. R., Lin, M., Xu, P., Wang, Z., Wang, X., Wen, L., Zhu, Y., Chen, T., Yang, L., Wang, Y., Chen, J., and Wang, W.: Significant increase of summertime ozone at Mount Tai in Central Eastern China, Atmos. Chem. Phys., 16(16), 10637-10650, **2016**.

Thornton, J.A., Wooldridge, P.J., Cohen, R.C., Martinez, M., Harder, H., Brune, W.H., Williams, E.J., Roberts, J.M., Fehsenfeld, F.C., Hall, S.R., and Shetter, R.E.: Ozone production rates as a function of NO_x abundances and HO_x production rates in the Nashville urban plume, J. Geophys. Res. - Atmospheres, 107(D12), doi.org/10.1029/2001JD000932, **2002**.

Wang, N., Guo, H., Jiang, F., Ling, Z. H., and Wang, T.: Simulation of ozone formation at different elevations in mountainous area of Hong Kong using WRF-CMAQ model, Sci. Total Environ., 505, 939-951, **2015b**.

Wang, T., Ding, A., Gao, J., and Wu, W. S.: Strong ozone production in urban plumes from Beijing, China, Geophys. Res. Lett., 33(21), **2006**.

Wang, T., Nie, W., Gao, J., Xue, L. K., Gao, X. M., Wang, X. F., Qiu, J., Poon, C. N., Meinardi, S., Blake, D., Wang, S. L., Ding, A. J., Chai, F. H., Zhang, Q. Z., and Wang, W. X.: Air quality during the 2008 Beijing Olympics: secondary pollutants and regional impact, Atmos. Chem. Phys., 10(16), 7603-7615, **2010**.

Wang, X. M., Lin, W. S., Yang, L. M., Deng, R. R., and Lin, H.: A numerical study of influences of urban land‐use change on ozone distribution over the Pearl River Delta region, China, Tellus B, 59(3), 633-641, **2007**.

Wang, Z., Li, Y., Chen, T., Zhang, D., Sun, F., Wei, Q., Dong, X., Sun, R., Huan, N., and Pan, L.: Ground-level ozone in urban Beijing over a 1-year period: Temporal variations and relationship to atmospheric oxidation, Atmos. Res., 164, 110-117, **2015a**.

1056 Whitten, G. Z., Heo, G., Kimura, Y., McDonald-Buller, E., Allen, D. T., Carter, W. P., and
1057 Yarwood, G.: A new condensed toluene mechanism for Carbon Bond: CB05-TU, Atmos.
1058 Environ., 44(40), 5346-5355, **2010**.

1059 Williams, J., Keßel, S.U., Nölscher, A.C., Yang, Y., Lee, Y., Yáñez-Serrano, A.M., Wolff, S.,
1060 Kesselmeier, J., Klüpfel, T., Lelieveld, J., and Shao, M.: Opposite OH reactivity and ozone
1061 cycles in the Amazon rainforest and megacity Beijing: Subversion of biospheric oxidant control
1062 by anthropogenic emissions, Atmos. Environ., 125, 112-118, **2016**.

1063 Willmott, C. J., Ackleson, S. G., Davis, R. E., Feddema, J. J., Klink, K. M., Legates, D. R.,
1064 O'Donnell, J., and Rowe, C. M.: Statistics for the evaluation and comparison of models, J.
1065 Geophys. Res. - Oceans, 90(C5), 8995-9005, **1985**.

1066 Xu, Z., Wang, T., Xue, L.K., Louie, P.K., Luk, C.W., Gao, J., Wang, S.L., Chai, F.H., and Wang,
1067 W.X.: Evaluating the uncertainties of thermal catalytic conversion in measuring atmospheric
1068 nitrogen dioxide at four differently polluted sites in China, Atmos. Environ., 76, 221-226, **2013**.

1069 Xue, L. K., Wang, T., Gao, J., Ding, A. J., Zhou, X. H., Blake, D. R., Wang, X. F., Saunders, S.
1070 M., Fan, S. J., Zuo, H. C., Zhang, Q. Z. and Wang, W. X.: Ground-level ozone in four Chinese
1071 cities: precursors, regional transport and heterogeneous processes, Atmos. Chem. Phys., 14(23),
1072 13175-13188, **2014**.

1073 Yang, Y., Shao, M., Wang, X., Nolscher, A.C., Kessel, S., Guenther, A., and Williams, J.:
1074 Towards a quantitative understanding of total OH reactivity: A review, Atmos. Environ.,
1075 134:147-161, **2016**.

1076 Yin, Y., Lu, H., Shan, W., and Zheng, Y.: Analysis of observed ozone episode in urban Jinan,
1077 China, Bulletin Environ. Contamination & toxico., 83(2), 159-163, **2009**.

1078 Zhang, Q., Streets, D. G., Carmichael, G. R., He, K. B., Huo, H., Kannari, A., Klimont, Z., Park,
1079 I. S., Reddy, S., Fu, J. S., Chen, D., Duan, L., Lei, Y., Wang, L. T., and Yao, Z. L.,: Asian
1080 emissions in 2006 for the NASA INTEX-B mission, Atmos. Chem. Phys., 9(14), 5131-5153,
1081 **2009**.

1082 Zhang, Q., Streets, D. G., He, K., Wang, Y., Richter, A., Burrows, J. P., Uno, I., Jang, C. J.,
1083 Chen, D., Yao, Z., and Lei, Y.: NO_x emission trends for China, 1995-2004: The view from the
1084 ground and the view from space, J. Geophys. Res. - Atmospheres, 112(D22), **2007**.

1085 Zhang, Q., Yuan, B., Shao, M., Wang, X., Lu, S., Lu, K., Wang, M., Chen, L., Chang, C. C., and
1086 Liu, S. C.: Variations of ground-level O_3 and its precursors in Beijing in summertime between
1087 2005 and 2011, Atmos. Chem. Phys., 14(12), 6089-6101, **2014**.

1088 Zhang, Y., Ding, A., Mao, H., Nie, W., Zhou, D., Liu, L., Huang, X., and Fu, C.: Impact of
1089 synoptic weather patterns and inter-decadal climate variability on air quality in the North China
1090 Plain during 1980-2013, Atmos. Environ., 124, 119-128, **2016**.

1091 Zhang, Z., Zhang, X., Gong, D., Quan, W., Zhao, X., Ma, Z., and Kim, S. J.: Evolution of
1092 surface O_3 and $PM_{2.5}$ concentrations and their relationships with meteorological conditions over
1093 the last decade in Beijing, Atmos. Environ., 108, 67-75, **2015**.

1094 Zhao, C., Wang, Y., and Zeng, T.: East China plains: A “basin” of ozone pollution, Environ. Sci.
1095 & Technol., 43(6), 1911-1915, **2009**.

1096 Zong, R., Yang, X., Wen, L., Xu, C., Zhu, Y., Chen, T., Yao, L., Wang, L., Zhang, J., Yang, L.,
1097 Wang, X., Shao, M., Zhu, T., Xue, L., and Wang, W.: Strong ozone production at a rural site in
1098 the North China Plain: Mixed effects of urban plumes and biogenic emissions, J. Environ. Sci.,
1099 doi.org/10.1016/j.jes.2018.05.003, **2018**.